May 31 (Thursday)

Plenary Lectures (Invited)

Oral presentations (Invited)

Oral presentations

PL-1 (Invited)

Functional high-yield molecular-scale electronic devices

Takhee Lee

Department of Physics and Astronomy, Seoul National University, Seoul 08826, Korea

E-mail: tlee@snu.ac.kr

Molecular electronics explores the intrinsic properties of materials at the molecular level and also may fulfill the increasing technical demands of the miniaturization of conventional silicon-based electronics. However, molecular electronics has suffered from a low device yield problem.

A simple vertically structured, metal-molecules-metal junctions were considered to be a general testbed for studying the charge transport characteristics of molecular junctions and their device applications, but the device yield of this method is very low because of metal filaments formed in the junctions during the fabrication process. To improve the yield, various methods have been proposed, such as by utilizing an intermediate protecting layer between the molecular layer and the top electrode, direct metal transfer, etc [2,3]. Using high yield methods, we were able to demonstrate functional molecular electronic devices. In this talk, I will give example studies [4]; (1) rectifying molecular electronic devices of ferrocene-alkanethiolate molecules which showed asymmetric electrical transport characteristics, and (2) photoswitching devices of diarylethene molecules which showed two electrical states (a high and a low conductance state) with a discrepancy of an order of magnitude when exposed to UV or visible light. In particular, these functional molecular devices were demonstrated not only on rigid substrates bur also on plastic flexible substrates.

References

[1]. D. Xiang et al. Chem. Rev. 116, 4318–4440 (2016).
[2]. Akkerman et al. Nature 441, 69 (2006); Wang et al. Adv. Mater. 23, 755 (2011).
[3]. Jeong et al. Nanotechnology 26, 025601 (2015); Jeong et al. Appl. Phys. Lett. 106, 063110 (2015).
[4]. Park et al. Nature Nanotech. 7, 438 (2012); Kim et al. Adv. Funct. Mater. 25, 5918 (2015); Kim et al. Adv. Funct. Mater. 24, 2472 (2014); Jeong et al. Adv. Mater. 26, 3968 (2014).

I1-1 (Invited)

Efficient and stable laser oscillation from organic semiconductor films

T. Matsushima[1-3], A. S. D. Sandanayaka[1,2], F. Bencheikh[1,2], K. Yoshida[1], M. Inoue[1], T. Fujihara[4], K. Goushi[1-3], J.-C. Ribierre[1,2], C. Adachi[1-3]*

[1]*OPERA, Kyushu University, 744 Motooka, Nishi, Fukuoka 819-0395, Japan.*
[2]*JST, ERATO, 744 Motooka, Nishi, Fukuoka 819-0395, Japan.*
[3]*WPI-I2CNER, Kyushu University, 744 Motooka, Nishi, Fukuoka 819-0395, Japan.*
[4]*ISIT, 5-14 Kyudai-shinmachi, Nishi, Fukuoka 819-0388, Japan.*

Tel: + 81 - 92 - 802 - 6923, Fax: +81- 92 - 802 - 6924
E-mail: tmatusim@opera.kyushu-u.ac.jp, adachi@cstf.kyushu-u.ac.jp

The demonstration of continuous-wave lasing from organic semiconductor films is highly desirable for practical applications in the areas of spectroscopy, data communication and sensing but it still remains a challenging objective. Here, we report low-threshold surface-emitting organic distributed feedback lasers operating in the quasi-continuous-wave regime at 80 MHz as well as under long pulse photoexcitation of 30 ms (Fig. 1) [1]. This outstanding performance was achieved using an organic semiconductor thin film with high optical gain, high photoluminescence quantum yield and no triplet absorption losses at the lasing wavelength combined with a mixed-order distributed feedback grating to achieve low lasing threshold. A simple encapsulation technique greatly reduced the laser-induced thermal degradation and suppressed the ablation of the gain medium taking place otherwise under intense continuous-wave photo-excitation. Overall, this study provides evidence that the development of a continuous-wave organic semiconductor laser technology is possible via the engineering of the gain medium and the device architecture.

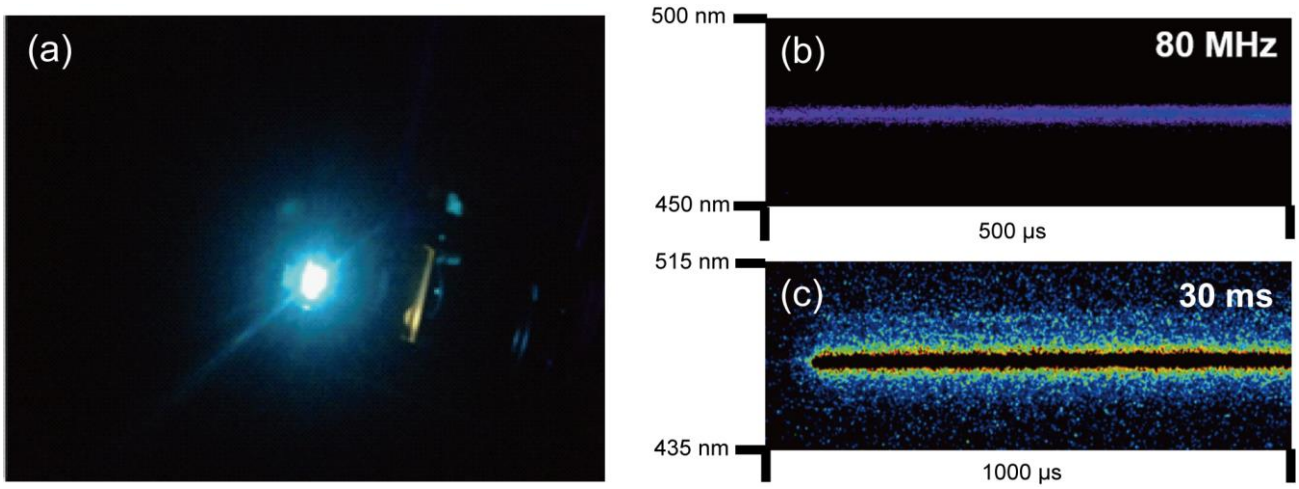

FIG. **1**. (a) Photograph of laser emission from our devices. Streak camera images of laser emission from devices operating at (b) 80 MHz and (c) 30 ms.

Reference

[1] A. S. D. Sandanayaka, T. Matsushima, F. Bencheikh, K. Yoshida, M. Inoue, T. Fujihara, K. Goushi, J.-C. Ribierre, and C. Adachi, Science Advances, **3**, e1602570, 2017.

I1-2 (Invited)

Organo-Lead-Halide Perovskite for Solar Cells and Light Emitting Applications by Chemical Vapor Deposition

Matthew R. Leyden,[1,2] Yabing Qi,[2] Chihaya Adachi[1]

[1] *Center for Organic Photonics and Electronics Research (OPERA), Kyushu University, 744 Motooka, Nishi, Fukuoka 819-0395, Japan*

[2] *Okinawa Institute of Science and Technology Graduate University 1919-1 Tancha, Onna-son, Kunigami-gun, Okinawa, Japan 904-0495*

Abstract

Organic metal halide perovskites are a set of materials with a rapidly increasing performance and broadening range of applications. The most widely known application of perovskite materials is solar cells,[1] where power conversion efficiencies have exceeded 22%.[2] There are a wide variety of fabrication methods for perovskite solar cells, but methods can be broadly grouped into the categories of solution deposition and vapor deposition.[3] Research on vapor deposited films make up a small fraction of the total research, but have also demonstrated impressive efficiencies of up to 20%.[4] This talk will focus specifically on chemical vapor deposition for perovskite solar cells.[5–7] Within the last few years perovskite materials have been gained interest in light emitting applications, such as light emitting diodes and optically driven lasers.[8,9] Light emitting diodes demonstrated an external quantum efficiency exceeding 10%,[10] and lasing thresholds below 1 μJ/cm^2.[11] Only a limited number of results have been published on light emitting diodes by vapor process. [12]

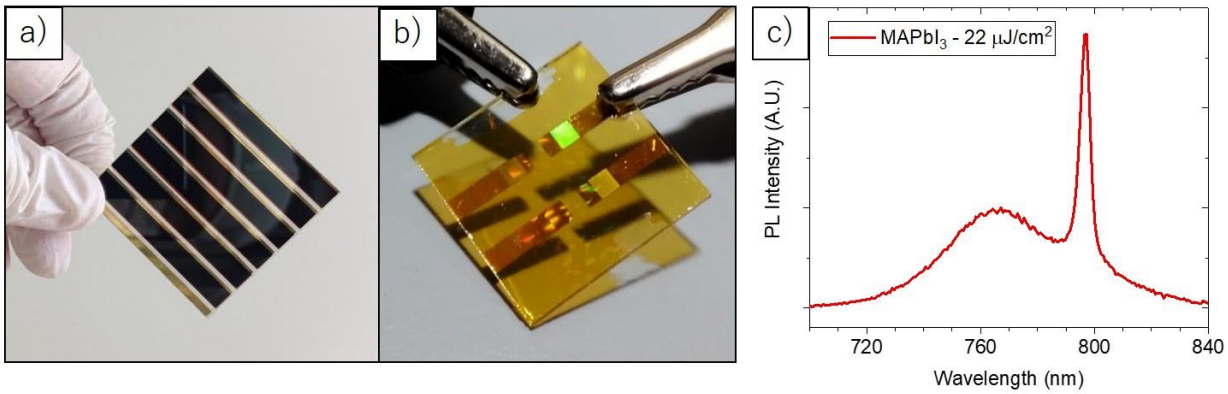

Figure. Example applications of organo-lead halide perovskite materials. a) Perovskite module fabricated by chemical vapor deposition. (5x5 cm, formamidinium lead iodide). c) A methylammonium lead bromide perovskite light-emitting diode prepared by chemical vapor deposition. c) Amplified spontaneous emission in methylammonium lead iodide.

References

[1] Grätzel, M. Acc. Chem. Res. 50, 487–491 (2017).

[2] Yang, W. S. et al. Science 356, 1376–1379 (2017).

[3] K. Ono, L., R. Leyden, M., Wang, S. & Qi, Y. J. Mater. Chem. A 4, 6693–6713 (2016).

[4] Momblona, C. et al. E Energy Environ. Sci. 9, 3456–3463 (2016).

[5] Leyden, M.R. et al. J. Mater. Chem. A 2, 18742–18745 (2014).

[6] Leyden, M.R., V. Lee, M., R. Raga, S. & Qi, Y. J. Mater. Chem. A 3, 16097–16103 (2015).

[7] Leyden, M.R., Jiang, Y. & Qi, Y. J. Mater. Chem. A 4, 13125–13132 (2016).

[8] Veldhuis, S. A. et al. Adv. Mater. 28, 6804–6834 (2016).

[9] Sutherland, B. R. & Sargent, E. H. Nat. Photonics 10, nphoton.2016.62 (2016).

[10] Xiao, Z. et al. Nat. Photonics 11 nphoton.2016.269 (2017).

[11] Saliba, M. et al. Adv. Mater. 28, 923–929 (2016).

[12] Leyden, M. R. et al, J. Phys. Chem. Lett. 8, 3193–3198 (2017).

I1-3 (Invited)

Vertical carrier transport in organic thin film devices

Ken-ichi Nakayama[1]

[1]*Department of Material and Life Science, Graduate School of Engineering, Osaka University, 2-1 Yamadaoka, Suita, Osaka 565-0871, Japan*
Tel: +81-6-6879-7368, Fax: +81-6-6879-7370
E-mail: nakayama@mls.eng.osaka-u.ac.jp

Organic electronic devices such as organic light-emitting diodes and organic solar cells generally have vertical device structure, where the organic semiconductor film is sandwiched by the two electrodes. The carrier mobility in perpendicular to the film surface (vertical direction) is important for improving the device performances, e.g. low voltage operation, high efficiency and high frequency response. In recent years, the lateral mobilities in organic field-effect transistors have been improved and high mobility exceeding 10 cm^2/Vs has been achieved. However, the vertical mobility of the organic thin film remains small value and there is a plenty of room for improvement (Fig. 1). In this presentation, we focus on carrier transport in a vertical direction in the organic thin film, and discuss materials design and controlling molecular arrangement to improve the vertical mobilities. Also some unique devices and materials application are introduced: high-performance vertical organic transistors named metal-base organic transistors[1], solution-processed organic solar cells using a photoprecursor method[2] and supramolecular materials. Furthermore, we discuss measurement method for mobility evaluation, and introduce CELIV (charge extraction by linearly increasing voltage) and its related method (Fig. 2) as a new standard technique for vertical mobility measurement[4].

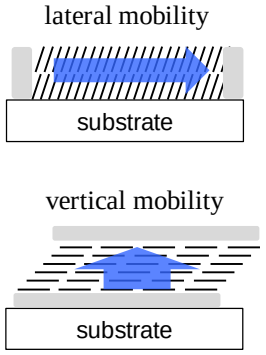

Fig. 1 Lateral and vertical device structure and ideal molecular arrangement for carrier transport.

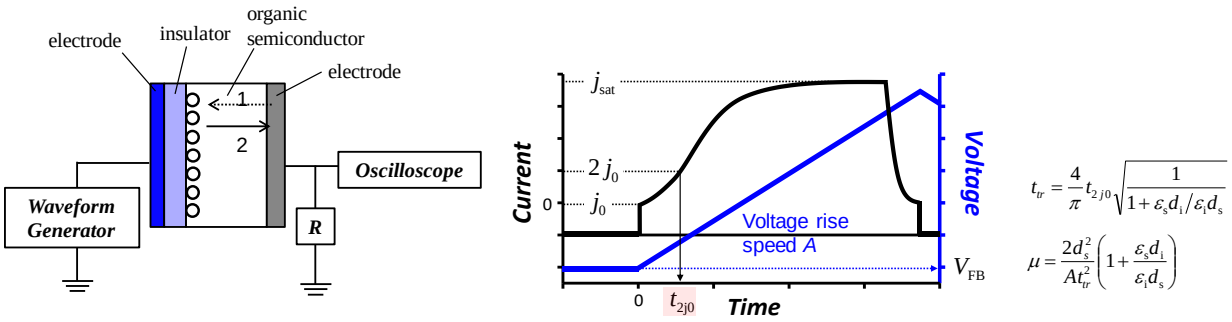

Fig. 2 Measurement setup and typical response for the MIS-CELIV measurement.

References

[1] K. Nakayama, S. Fujimoto, and M. Yokoyama, "High-current and low-voltage operation of metal-base organic transistors with LiF/Al emitter", *Appl. Phys. Lett.*, **88**, 153512 (2006).
[2] K. Takahashi, D. Kumagai, N. Yamada, D. Kuzuhara, Y. Yamaguchi, N. Aratani, T. Koganezawa, S. Koshika, N. Yoshimoto, S. Masuo, M. Suzuki, K. Nakayama, H. Yamada, "Side-chain engineering in a thermal precursor approach for efficient photocurrent generation", *J. Mater. Chem. A*, **5**, 14003-14011 (2017).
[3] K. Yamada, Y. Suwa, C. Katagiri, and K. Nakayama, "High vertical carrier mobility in the nanofiber films of a phthalocyanine derivative and its application to vertical-type transistors", *Org. Electron.*, **53**, 320-324 (2018).
[4] C. Katagiri and K. Nakayama, "Charge carrier mobility evaluated from extraction current transients and space-charge-limited current in poly(3-hexylthiophene) thin film ", *Appl. Phys. Express*, **11**, 011601-1-4 (2018).

I1-4 (Invited)

Relationships between structure and charge transfer kinetics at organic monolayer/oxide interfaces probed using waveguide spectroelectrochemistry – toward understanding and enhancing the efficiency of organic electronic devices

S. Scott Saavedra

Department of Chemistry and Biochemistry, University of Arizona, 1306 E. University Tucson, AZ 85721-0041 USA
Tel: + 1 – 520-621-9761 Fax: + 1 – 520-621-8407
E-mail: saavedra@email.arizona.edu

Charge transfer efficiency at organic/electrode interfaces in organic photovoltaic (OPV) devices and organic light emitting diodes (OLEDs) can be an important parameter in overall device performance. Rates of charge transfer across these interfaces are determined by a number of factors, such as offsets in frontier orbital energies, wave function overlap, reorganization energies, and charge mobilities, which in turn depend on structural parameters, e.g. packing and orientation, of the interfacial molecular layers. Modification of the electrode/donor interface with a redox-active, organic surface modifier may enhance charge injection across the interface by providing a facile electron transfer pathway between the contact and the adjacent organic layer, and by controlling chemical and physical interfacial compatibility and the effective work function of the contact. We are developing and implementing spectroelectrochemical approaches to study relationships between molecular structure and electron transfer kinetics in monolayers of redox-active chromophores tethered to transparent conducting oxide electrodes, where the monolayer is a model for the interfacial layer in an OPV or OLED.

This talk will highlight studies of phthalocyanines and perylenes tethered to indium-tin oxide (ITO) using a novel form of electroreflectance spectroscopy, potential-modulated, attenuated total reflection spectroscopy (PM-ATR). In PM-ATR, the intensity of visible light propagating in a planar waveguide electrode coated with ITO is monitored while an ac potential modulation is simultaneously applied to the ITO layer. The evanescent field at the surface of the waveguide interacts with an overlying thin film of redox-active chromophores. Changes in the absorbance of the film as a function of the light polarization, modulation frequency, and amplitude provide information about electron transfer rates and molecular structure.

References

[1] Y. Zheng and S. Scott Saavedra, "Characterization of Charge Transfer Kinetics at Organic/Electrode Interfaces Using Potential-Modulated Attenuated Total Reflectance (PM-ATR) Spectroscopy," Anal. Sci., vol.33, pp.427-433, 2017.

I1-5 (Invited)

Integrated synthesis of graphene nanoribbons toward high performance optoelectrical devices

Toshiaki Kato[1,2], Toshiro Kaneko[1]

[1] *Department of Electronic Engineering, Tohoku University,*
6-6-05 Aoba, Aramaki, Aoba-ku, Sendai, 980-8579 Japan
[2] *JST-PRESTO*
Tel: + 81 - 22 - 795 - 7046, Fax: +81- 22 -263 - 9225
E-mail:kato12@ecei.tohoku.ac.jp

Graphene nanoribbons (GNRs) combine the unique electronic and spin properties of graphene with a transport gap that arises from quantum confinement and edge effects. This makes them an attractive candidate material for the channels of next-generation transistors. However, the reliable site and alignment control of nanoribbons with high on/off current ratios remains a challenge. We have developed a new, simple, scalable method based on novel plasma catalytic reaction [1-5] for directly fabricating narrow GNRs devices with a clear transport gap [6]. Since the establishment of our novel GNR fabrication method, direct conversion of a Ni nanobar to a suspended GNR is now possible. Indeed, GNRs can be grown at any desired position on an insulating substrate without any post-growth treatment, and the wafer-scale synthesis of suspended GNR arrays with a very high yield (over 98%) is realized [7]. The growth dynamics of suspended GNR is also investigated through the systematic experimental study combined with molecular dynamics simulation and theoretical calculations for phase diagram analysis. The improvement of thermal stability of Ni nanobar can be a key to realize the GNR nucleation in our method, which can be given by supplying higher density of carbon from plasma to liquid-phase Ni nanobar. The wettability of liquid-phase Ni nanobar against to the SiO_2 substrate is also found to be an important factor forming the suspended structure of GNR. It is also revealed that the minimum length of GNR can be decided by the wavelength of Plateau-Rayleigh instability known as a traditional instability of fluid flow. We believe that our results can contribute to pushing the study of atomically thin layered materials from basic science into a new stage related to the optoelectrical applications [8-10] in industrial scale.

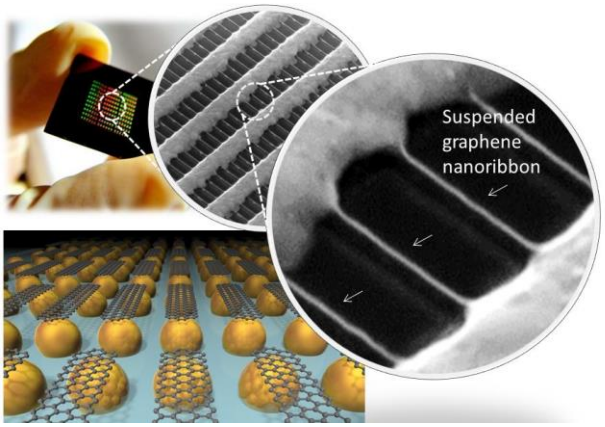

Figure 1: Large-scale integration of suspended GNR arrays.

References

[1] T. Kato and R. Hatakeyama,"Exciton Energy Transfer Assisted Photoluminescence Brightening from Freestanding Single-Walled Carbon Nanotube Bundles", J. Am. Chem. Soc., vol. 130, no. 25, pp. 8101-8107, May 2008.

[2] T. Kato and R. Hatakeyama, "Direct Growth of Short Single-Walled Carbon Nanotubes with Narrow-Chirality Distribution by Time-Programmed Plasma Chemical Vapor Deposition", ACS Nano, vol. 4, no.12, pp 7395-7400, Nov. 2010.

[3] T. Kato and R. Hatakeyama,"Direct Growth of Doping-Density-Controlled Hexagonal Graphene on SiO_2 Substrate by Rapid-Heating Plasma CVD", ACS Nano, vol. 6, no. 10, pp. 8508-8515, 2012.

[4] T. Kato and R. Hatakeyama, "Direct Growth of Short Single-Walled Carbon Nanotubes with Narrow-Chirality Distribution by Time-Programmed Plasma Chemical Vapor Deposition", ACS Nano, vol. 4, no.12, pp. 7395-7400, Nov. 2010.

[5] B. Xu, T. Kaneko, Y. Shibuta, T. Kato, "Preferential synthesis of (6,4) single-walled carbon nanotubes by controlling oxidation degree of Co catalyst", Scientific Reports, vol. 7, no. 11149, pp. 1- 9, Sep. 2017.

[6] T. Kato and R. Hatakeyama, "Site- and alignment-controlled growth of graphene nanoribbons from nickel nanobars", Nature Nanotechnology, vol. 7, no. 10, pp. 651-656, Sep. 2012.

[7] H. Suzuki, T. Kaneko, Y. Shibuta, M. Ohno, Y. Maekawa, and T. Kato, "Wafer scale fabrication and growth dynamics of suspended graphene nanoribbon arrays", Nature Communications, vol. 7, no. 11797, pp. 1-10, Jun 2016.

[8] T. Kato and T. Kaneko, "Optical Detection of a Highly Localized Impurity State in Monolayer Tungsten Disulfide", ACS Nano, vol. 8, no. 12, pp. 12777-12785, Dec. 2014.

[9] T. Akama, W. Okita, R. Nagai, C. Li, T. Kaneko, T. Kato, "Schottky solar cell using few-layered transition metal dichalcogenides toward large-scale fabrication of semitransparent and flexible power generator", Scientific Reports, vol. 7, no. 11967, pp. 1-10, Sep. 2017.

[10] T. Kato and T. Kaneko, "Transport Dynamics of Neutral Excitons and Trions in Monolayer WS2", ACS Nano, vol. 10, no. 10, pp. 9687-9694, Sep. 2016.

I1-6 (Invited)

Flexible organic light-emitting diodes based on stacked and surface-modified transparent conducting oxides

Ching-Ming Hsu, Wen-Tuan Wu, Don-Han Tsai and U-Jun Peng

Department of Opto-Electrical Engineering, Southern Taiwan Uni. of Science and Technology, 1, Nan-Tai St., Yung-Kang Dist., Tainan City, 710 Taiwan
Tel: + 886 - 6 -2533131, Fax: +886-63 -243-2912
E-mail:tedhsu@stust.edu.tw

Flexible organic light-emitting diodes (OLEDs) have shown their great potentials in next generation display and lighting applications. Mechanical flexibility is a great concern when flexible OLEDs employ a transparent conducting oxide (TCO) as their electrodes. This is because TCOs are naturally brittle and can crack under a high strain, resulting in electrical degradation of OLEDs. For this reason, a variety of alternative materials such as AgNWs [1], thin metallic films [2], conducting polymers [3] and hybrid materials [4] have been brought to replace TCOs. However, the use of these alternatives may be at expense of high manufacturing cost, deteriorated optical transmittance and device reliability. This article reports how a FOLED can operate with stacked and surface-modified TCOs and discusses their possibility for FLOED applications.

To form a stacked structure indium tin oxide (ITO), 150 nm thick commercially coated on PET, was bent at a curvature of 6 mm in radius to intentionally create cracks on ITO film. The cracked film was sputter coated with a 20-nm-thick ITO in order to fill the cracks. Another bending followed to yield cracks on the second ITO film. A top ITO of 20 nm was deposited to fill the cracks again, and it was thermally annealed at 150 ^{o}C for 1 h to improve the optical and electrical characteristics of the stacked ITO film. To form surface-modified structures an initial of ITO on PET was recessed to a depth of 50 nm. The fabrication process of recesses can be seen elsewhere [5]. Basically, the process was to generate circular recesses with a recess coverage ratio of 7.9%, 14.1%, 20.9% and 27.7% on ITO surfaces. OLEDs were fabricated on both types of ITO anodes. The electrical, optical and flexibility performances of the stacked and surface-modified ITO were examined. Device characteristics based on these ITO anodes were compared with those with a traditional ITO electrode.

Table 1 gives the changes in electrical sheet resistance and optical transmittance of ITO after being processed with the stacking and recessing schemes. The optical transmittance shown is with and without a PET substrate counted for recessed and stacked films, respectively. The table also shows the ITO film resistance variation ratio (R/Ro) after a 400-cycle bending test at r = 14 mm to represent the degree of mechanical flexibility. It clearly reveals there is around 10% increase of electrical resistance for both stacked and recessed films, while the optical transmittance approximately remains unchanged. This indicates the stacked and recessed structures yield no apparent negative effects on electrical and optical properties of ITO film. Interestingly, we found the stacked and recessed structures seemed to improve the mechanical flexibility with R/Ro drops from 2.6 to 2.3 and 3.1 to 1.9, respectively. The large drop of R/Ro for the 7.9% recessed film suggests that the flexibility of ITO can be greatly reinforced at a specific recess pattern.

Figure 1 shows the luminance–voltage (L-V) characteristic of an OLED with the stacked ITO anode in comparison with that with the traditional ITO anode. It clearly discovers that the OLED device fabricated on the stacked ITO anode exhibits degraded illumination. It is likely the additionally coated ITO cannot fully fill the intentionally generated cracks, leaving locally deformed areas where relatively low electrical current flows. Fig. 2 compares the L-V characteristics of ITO-recessed OLEDs with that having a planar ITO anode. One can see all ITO-recessed OLEDs perform enhanced illumination at the same driven voltages with the largest increment of 166% at 10 V for the 27.7% recessed device. This is mainly attributed to the enhanced light extraction in the presence of these recesses. We found the light extraction enhancement mechanism for recessed ITO on PET is different from that on glass substrate, and will further examine it.

In conclusion, this study demonstrates that it is possible to improve mechanical flexibility of a TCO film using both multiple film stacking and surface-recessing schemes. Initial results show that OLEDs fabricated on stacked TCO anodes exhibited degraded characteristics probably due to uncompleted crack filling. More work is to be done to optimize the quality of the stacked film. On the other hand, OLEDs fabricated on recessed TCO anodes performed considerably improved characteristics as a result from enhanced light extraction by the recesses. Optimization on recess physical dimensions in the following study to reach a high mechanical flexibility and a highly efficient OLED device is necessary.

Table 1 Electrical, optical and mechanical performances of stacked and recessed ITO films

	Stacking Scheme			Recessing Scheme				
	initial ITO	cracked ITO	stacked ITO	initial ITO	7.9% r-ITO	14.1% r-ITO	20.9% r-ITO	27.7% r-ITO
Sheet Resistance (Ω/□)	60	230	65	55.4	60.1	60.9	63.2	66.2
Optical Transmittance (%)	90.2	93.2	91.7%	79.7	79.4	79.2	79.3	79.3
Resistance Variation, R/Ro	2.6	--	2.3	3.1	1.9	2.5	2.8	2.9

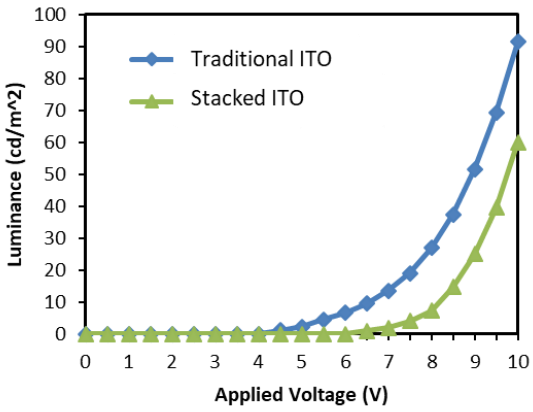

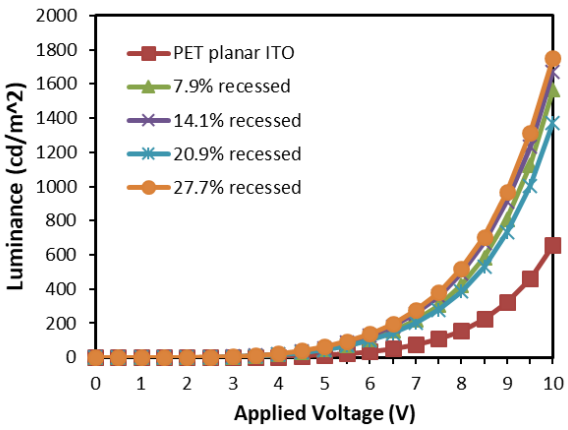

References

[1] W. Kerk , and C. Wong, "Transparent conductive film by large area roll-to-roll processing", Thin Solid Films, vol. 544, pp.427–432, 2013.

[2] M. Kawamura, Y. Ishizuka, S. Yoshida, Y. Abe, and K. Kim "Ag thin film on an organic silane monolayer applied as anode of organic light emitting diode", Thin Solid Films, vol. 532, pp. 7–10, 2013.

[3] D. Cairns, and G. Crawford, "Electromechanical Properties of Transparent Conducting Substrates for Flexible Electronic Displays", Proc. IEEE, vol. 93(8), pp. 1452-1457, 2005.

[4] J. Liang, L. Li, K. Tong, Z. Ren, W. Hu, X. Niu, Y. Chen, and Q. Pei, "Silver nanowire percolation network soldered with graphene oxide at room temperature and its application for fully stretchable polymer light-emitting diodes", ACS Nano, vol. 8, 1590-1600, 2014.

[5] C.M. Hsu, Y.X. Zeng, B.T. Lin, W.M. Lin, and W.T. Wu, "Enhanced Light Extraction of Organic Light-emitting Diodes Using Recessed Anodes", Appl. Surf. Sci., vol. 309, pp. 33-37, 2014.

PL-2 (Invited)

Flexible Printed Organic Electronics Technology and Wireless IoT Sensor Applications

Shizuo Tokito

Research Center for Organic Electronics, Yamagata University
4-3-16, Jonan, Yonezawa, Yamagata, 992-8510 Japan
Tel: +81 - 238 – 26 - 3725, Fax: +81- 238 -26 - 3788
E-mail: tokito@yz.yamagata-u.ac.jp

1. Introduction

Flexible printed organic electronics technology has been garnering increasing attention in research and development because of its potential for low-cost, environmentally-friendly electronic devices in new applications employing flexible form factors. In particular, there is an immense need to deploy sensor frameworks for the so-called Internet of Things (IoT). These applications are envisaged as thin-film transistor (TFT) devices with various types of sensors fabricated using a variety of printing processes on thin plastic film substrates. Here, TFT devices based on organic semiconductor (OSC) materials can be fabricated at low temperatures and are more compatible with printing methods and low-cost plastic substrates than inorganic semiconductors. Therefore, printed organic TFT (OTFT) devices are expected to have great potential in these applications.

Here, we report briefly on recent advancements in printable electronic materials, printed OTFT devices used in integrated circuits and IoT sensor applications. Existing silicon LSI technology was also employed in these sensor applications, an approach called 'Flexible Hybrid Electronics'.

2. Printable Electronic Materials

Silver (Ag) nanoparticle inks have become important materials for the fabrication of electrode and interconnect layers in printed electronics. Accordingly, we developed an Ag nanoparticle ink that was optimized for organic TFT applications. Finely patterned Ag lines with line widths of 39 -100 μm were fabricated by inkjet printing and sintered at temperatures lower than those reported for other Ag nanoparticle inks. A low resistivity of less than 10 μΩ-cm could be attained in the printed lines by thermal sintering at 120° C or with photonic sintering for 1 msec.

We adopted a newly developed p-type OSC material based on a dithienobenzodithiophene derivative (DTBDT), which is soluble in common organic solvents and highly crystalline. During OTFT device fabrication, the surfaces of the source and drain were treated with self-assembled monolayer (SAM) materials to reduce the contact resistance. A high carrier mobility of 3 cm^2/Vs and a high on/off current ratio of 10^7 were obtained in a typical bottom-contact top-gate OTFT device. A new n-type OSC material, 'TU series', based on a benzobisthiadiazole moiety was also developed for CMOS inverter circuits. A mobility of 1 cm^2/Vs was demonstrated in a top-contact bottom-gate OTFT device.

3. Printed OTFT Devices & Integrated Circuits

Inkjet printing, nozzle dispensing and reverse-offset printing as well as spin-coating methods were employed in forming the electrodes, bank and OSC layers, resulting in fully-printed or nearly fully-printed OTFT devices. By optimizing the OSC ink formulation and thermal annealing of the OSC layer, excellent p-type electrical performance with a high mobility over 1 cm^2/Vs and a high on/off current ratio of over 10^7 were achieved at a low operating voltage.

The important applications of OTFT devices are integrated circuits for RFID devices and in microprocessors. We successfully fabricated pseudo-CMOS inverters using p-type OTFT devices, as well as NAND logic gates, which exhibited ideal characteristics at low operating voltages and very high gains of over 250. More recently, we have succeeded in fabricating a six-stage ring oscillator with ultra-low voltage operation of around 0.3 V, which was driven by a biofuel cell with an output voltage of 0.4 V.

True CMOS inverters using both p-type and n-type OSC materials are important for low-power, high-speed operation, and for circuit designs with compact layouts. Using our n-type OSC material (TU-3) and a commonly used p-type OSC material (diF-TES ADT), we fabricated a CMOS inverter that employed a stacked TFT device construction. Good switching characteristics were observed and a high gain was obtained at an operating voltage of 10 V.

Based on this CMOS inverter design, three–stage ring oscillator and D-flip flop circuits were also fabricated. To increase the compactness of these circuits, clocked inverters were employed, resulting in about a 50% reduction in the transistor count and circuit area.

In order to realize very short-channel OTFT devices and higher performance integrated circuits, we employed the reverse-offset printing method to form narrow channel lengths below 10 μm, resulting in good electrical characteristics for printed CMOS inverter and operational amplifier circuits.

4. OTFT Based Sensors

We employed an OTFT device as the transducer for various sensors such as physical and chemical sensors. The detection signals can be obtained electrically, which is convenient for signal processing and wireless transmission. Moreover, a pressure sensor based on ferroelectric polymer (PVDF-TrFE) materials is superior in detecting vital signals for the human body. We previously succeeded in clear detection of pulse wave in wearable patch type sensor, which was fabricated on a plastic film substrate using printing methods. In order to employ these in healthcare applications, a cold chain temperature sensor was developed using a conductive polymer, PEDOT:PSS, in which conductivity has a temperature dependence. We have also reported on the detection of biomarkers related to various infectious diseases and illnesses using a similar sensor configuration. The basic biosensor construction consists of an OTFT device with an extended gate electrode, upon which receptors are immobilized. Immunoglobulin A and Glucose were successfully detected in an aqueous solution using the organic transistor-based biosensors.

5. IoT Sensor Applications

Our goal is to develop a smart sensor device, which combines printed integrated circuits and a sensor, and can be connected wirelessly to the Internet. The integrated circuits are operational amplifier, I-V converter, A/D converter etc. The pseudo-CMOS inverters were used for amplifier and potential control of reference electrode in a lactate sensor, and K ion sensor. Excellent signal amplification and current-voltage conversion were demonstrated. A three-stage amplifier was prepared on the same plastic film substrate with a sensor, and an amplification of 10 times was observed in the printed pressure sensor.

More recently, we are developing flexible hybrid sensors, whereby silicon-based LSI die are used for the signal processing and wireless communication circuits and integrated onto a flexible plastic film substrate. The sensors, interconnects, and antenna are patterned with screen printing or inkjet printing, after which Si-LSI die and resistors are mounted on the same film substrate. Both Near Field Communication (NFC) or Bluetooth Low Energy (BLE) protocols are used for wireless communication. A wearable temperature sensor was successfully demonstrated by employing a PEDOT:PSS sensor element.

References

1. K. Fukuda, et al., Organic Electronics 13, 1660 (2012).
2. Y. Takeda, et al., Organic Electronics 14, 3362 (2013).
3. K. Fukuda, et al., Nature Commun. 5, 243703 (2014).
4. Y. Yoshimura, et al., Organic Electronics 15, 2696 (2014).
5. Y. Takeda, et al., Jpn. J. Appl. Phys. 54, 04DK03 (2015).
6. K. Fukuda, et al., Adv. Electro. Mater. 1, 1400052 (2015).
7. K. Fukuda, et al., Adv. Electro. Mater. 1, 1500145 (2015).
8. M. Mamada, et al., Chem. Mater. 27, 141 (2015).
9. Y. Takeda, et al., Scientific Reports 6, 25714 (2016).
10. R. Shiwaku, et al., Scientific Reports 6, 34723 (2016).
11. J. Kwon, et al., ACS Nano, DOI :10.1021 /acsnano.6b06041 (2016).
12. R. Shiwaku, et al., Adv. Electron. Mater. 3, 1600557(2017).
13. K. Hayasaka, et al, Adv. Electron. Mater. 3, 1700208(2017).
14. T. Minamiki, et al., Materials 7, 6843 (2014).
15. T. Minami, et al., Chem. Commun. 50, 15613 (2014).
16. T. Minamiki, et al., Analytical Sciences 31, 725 (2015).
17. T. Minami, et al., Biosens. Bioelectron. 81, 87 (2016).

I2-1 (Invited)

Flexible IoT Sensor Device Fabrication Using Advanced Low-damage Manufacturing Techniques

Toshihide Kamata, Taiki Nobeshima, Shusuke Kanazawa, Sei Uemura,
Manabu Yoshida and Hirobumi Ushijima

Flexible Electronics Research Center, AIST,
1-1-1 Higashi, Tsukuba-shi, Ibaraki, 305-8565 Japan
Tel: + 81 - 29 - 861 - 4516, Fax: +81- 29 - 849 - 1047
E-mail: t-kamata@aist.go.jp

Recently, flexible electronics is one the most active technology area in the electronics, and many have been trying to develop several types of flexible devices such as a flexible sensor, a flexible display, a flexible actuator, a flexible circuit, and a flexible battery. It has been well recognized that development of low-damage device manufacturing technology is important to prepare such a flexible device. Especially, in order to prepare a IoT device such as mobile, wearable, portable sensor devices, several kinds of low damage manufacturing technologies are required to keep the performance of a device with customized design, such as light weight, free shape design, compact mounting and so on. In this talk, our newly developed low-damage manufacturing technologies, and flexible IoT sensor devices prepared by the low-damage manufacturing technologies will be introduced.

Flexible devices are usually prepared on a flexible and/or soft material substrate to show its device mechanical flexibility. In many cases during the flexible device manufacturing, several kinds of process stress such as thermal stress, mechanical stress and chemical stress are applied on the device, which often destroy the device performance easily. We have developed a unique print technology with a combination of offset printing and rapid drying to reduce a mechanical stress and chemical stress. One is classified as a soft MEMS technology which enable us to form a bridge structure even on a soft material substrate such as plastic substrate, textile and soft sponge materials. By applying the technology, we have succeeded in development of a respiration sensor with a cantilever system on a soft sponge material of a headset microphone, which are applied to check health condition of a driver.

Several types of stretchable device materials have been also developed. IoT devices are often required to put it on a unique shape surface. If the surface is formed undevelopable surface shape, conventional flexible device can not be put on it because it is formed with developable surface. In this case, stretchable device is required to prepare for covering the undevelopable surface. The unique point of our developed stretchable device materials is in its tunability of the sensitivity of resistivity change to the stretch. Some stretchable device material has high sensitivity of its resistivity change to the deformation of the pattern. It is well applicable to the pressure sensor with high sensitivity. By using these materials, large scale stretchable IoT sensor was developed, which is applicable to the seat sensor, grip sensor, air current sensor and so on. Study of these device design will be introduced.

(a) (b)

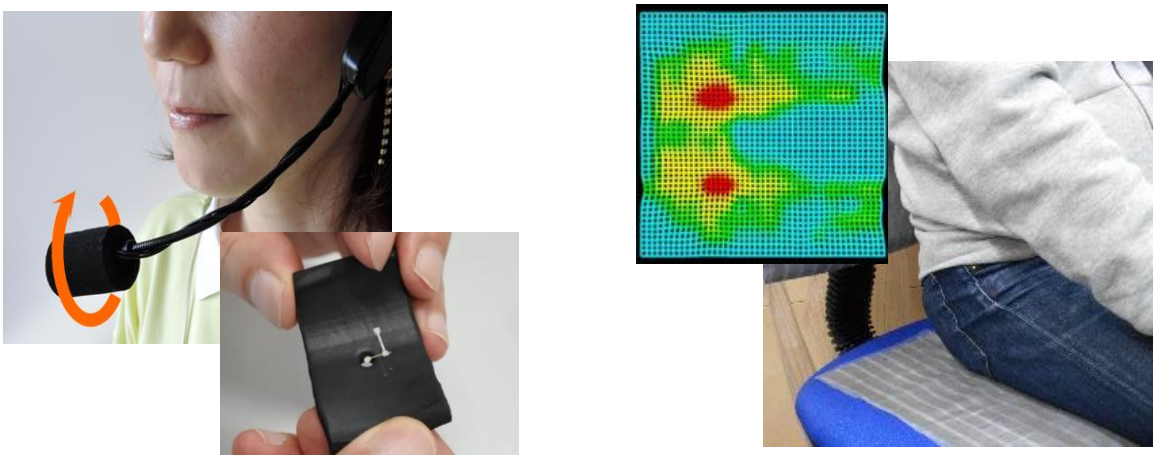

Fig.1 (a) Flexible respiration sensor prepared on a sponge substrate by newly developed low-damage print techniques. (b) Stretchable sheet sensor for detecting pressure distribution on a seat.

I2-2 (Invited)

Ultraflexible organic solar cells: approaches to high performance and stable operation

Kenjiro Fukuda1,2, Hiroaki Jinno1,3, Xiaomin Xu1, Sungjun Park1, and Takao Someya1,2,3

1 RIKEN Center for Emergent Matter Science
2-1 Hirosawa, Wako, Saitama, 351-0198 Japan
Tel: + 81 - 48 - 467 - 9174, Fax: 81 - 48 - 467 – 5348
2 Thin-Film Device Laboratory, RIKEN
3 Electrical and Electronic Engineering and Information System, The University of Tokyo
E-mail:kenjiro.fukuda@riken.jp

Ambient power under a harsh environment can significantly expand the applications of sensors and electronics for Internet of things (IoT). Indeed, wearable IoT sensors need extraordinarily durable power sources with mechanical durability and environmental stability. Although photovoltaic cells are promising power sources to supply sufficient electricity (order of mW) to IoT sensors and e-textiles, environmental stability. We are trying to solve these problems from various view point by checking each material itself and process, both high power conversion efficiency and high stability can be achieved. To date, we have achieved ultra-flexible organic solar cells with high power conversion efficiency (up to 10%), water-proof properties [1], thermal-stability [2], and mechanical robustness [3] (Figure 1). In this talk, we will discuss how to achieve such high efficient and stable solar cells on ultraflexible substrates.

[1] H. Jinno, K. Fukuda, X. Xu, S. Park, Y. Suzuki, M. Koizumi, T. Yokota, I. Osaka, K. Takimiya, and T. Someya, “Stretchable and waterproof elastomer-coated organic photovoltaics for washable electronic textile applications,” *Nat. Energy*, vol. 2, no. 10, pp. 780–785, Oct. 2017.

[2] X. Xu, K. Fukuda, A. Karki, S. Park, H. Kimura, H. Jinno, N. Watanabe, S. Yamamoto, S. Shimomura, D. Kitazawa, T. Yokota, S. Umezu, T.-Q. Nguyen, and T. Someya, “Thermally stable, highly efficient, ultraflexible organic photovoltaics,” *Proc. Natl. Acad. Sci.*, doi: 10.1073/pnas.1801187115, Apr. 2018.

[3] and T. S. Z. Jiang, K. Fukuda, X. Xu, S. Park, D. Inoue, H. Jin, M. Saito, I. Osaka, K. Takimiya, and T. SomeyaZ. Jiang, K. Fukuda, X. Xu, S. Park, D. Inoue, H. Jin, M. Saito, I. Osaka, K. Takimiya, “Reverse-Offset Printed Ultrathin Ag Mesh for Robust Conformal Transparent Electrodes for igh-Performance Organic Photovoltaics,” *Adv. Mater.*, doi: 10.1002/adma.201707526, 2018.

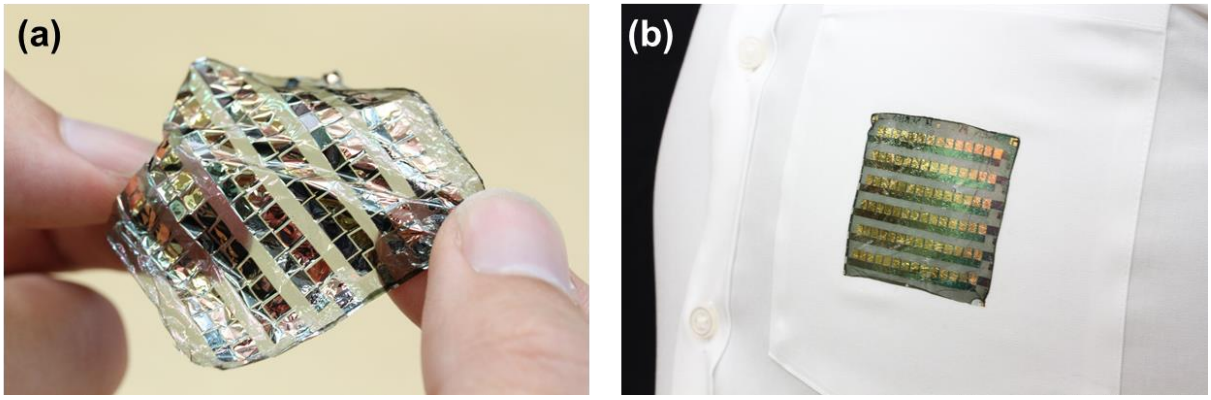

Figure 1: Ultraflexible organic solar cells. (a) A photograph of freestanding ultraflexible organic solar cells. The thickness is only 3 μm including substrates and passivation layers. (b) Because of high thermal stability, our solar cells can be adhered onto clothes with hot-melt process without degradation of performances.

O3-1

Tip-unenhanced Raman scattering

Saki Nakae, Kazuhiro Miyashita, Masayuki Futamata*

Graduate School of Science and Engineering, Saitama University,
255Shimo-okubo, Sakura-ku, Saitama, 338-8570 Japan
**Tel: + 81 - 48 - 858 – 3383, *E-mail: futamata@chem.saitama-u.ac.jp*

A gap mode in a configuration of metal nanoparticles (MNPs)/adsorbates/metal substrates has been developed in surface enhanced Raman scattering (SERS) [1-10]. In this geometry, a coupling of dipoles in metal nanoparticles (MNPs) generated by localized surface plasmon (LSP) and image dipoles induced in metal substrates provides enormously enhanced electric field at a nanogap where adsorbates are located. Metiu et al. [1] analyzed enhanced electric field at a nanogap between MNPs and metal substrates in early ’80s with respect to the enhancement mechanism of SERS. Even single crystals of gold with different surface indices are available in the gap mode to elucidate their distinct adsorption properties [4]. Yet details in a gap mode have not been reported, for instance how the enhancement factor depends on dielectric constants of substrates, and also on size of MNPs. Therefore, we investigated these issues using finite difference time domain (FDTD) calculations and SERS measurements.

In a gap mode under external geometry, we found that various metal substrates with large damping including Pb, Sn, Cu, Zn, Al, and Pt are available [5, 8]. Note that these metal substrates, which were not effective in early stage of SERS history using their roughened surfaces exploiting localized surface plasmon (LSP), provided markedly enhanced electric field of 10^5-10^7 at a nanogap by immobilizing AuNPs with a radius (r_{AuNP}) of 15 nm. These features are explained by the aforementioned coupling of dipoles in AuNPs and their image dipoles in the substrates. Hence, not only metal substrates but also dielectrics with sufficiently large optical constants compared to surrounding media. For instance, Si substrates with dielectric constants larger than 10 at 632 nm provided pronounced enhancement of ~10^6 in SERS. Also, the larger size of an AuNP provided the larger enhancement in electric field at a nanogap, as exemplified by 5.2×10^3 at r_{AuNP}= 15 nm to 3.8×10^4 at r_{AuNP}=50 nm on Zn substrate. Correspondingly, SERS measurements yielded the larger enhancements of 10^7-10^8 for the larger AgNPs (50 nm) than those (10^4-10^5) for smaller particles (15 nm) on Pb, Zn, Ni and Pt substrates. Thus, we confirmed that a gap mode is available not only for various transition metals with large damping, but also for dielectric materials with large optical constants, and larger enhancement factor for larger AuNPs.

We further investigated a gap mode with inverse geometry, namely XNPs/adsorbates/Ag or Au substrates. Here, the symbol of XNPs denotes non-metal nanoparticles with large dielectric constants like Si or TiO_2. Even in this geometry, inherently similar multiple coupling of dipoles generated in XNP and image dipoles or those via PSP in metal substrates may give rise to marked electric field at a nanogap. We indeed obtained Raman enhancement of 10^5-10^6 for TP on Ag substrates after immobilization of SiNPs and TiO_2 NPs in agreement with FDTD calculations. These results are promising to exploit a gap mode Raman spectroscopy of elucidating surface chemistry on various functional materials and also to realize TERS with using a naked Si cantilever. Indeed, we recently confirmed that photocatalytic degradation of methylene blue can be monitored using a gap mode between TiO_2 NPs and Ag substrates [11]. Also, we confirmed that a naked Si cantilever gives promising enhancement in Raman signal intensity of ~10^5 for TP adsorbed on Ag substrates under attenuated total reflection (ATR) geometry [11].

References

[1] P. K. Aravind and H. Metiu, “The effects of the interaction between resonances in the electromagnetic response of a sphere-plane structure; applications to surface enhanced spectroscopy”, *Surf. Sci.* 1984, 124, 506. [2] M. Futamata, Y. Maruyama, and M. Ishikawa, “Thermal Activation of Blinking in SERS Signal”, *J. Phys. Chem. B* 2004, 108, 13119. [3] K. Kim, H. B. Lee, J. Y. Choi and K. S. Shin, “Characteristics of Nanogaps Formed by Planar Au and Pt Nanoparticles Revealed by Raman Spectroscopy”, *J. Phys. Chem. C* 2012, 115, 21047. [4] K. Ikeda K, K. Takahashi, T. Masuda, H. Kobori, M. Kanehara, T. Teranishi and K. Uosaki, “Structural Tuning of Optical Antenna Properties for Plasmonic Enhancement of Photocurrent Generation on a Molecular Monolayer System”, *J. Phys. Chem. C 2012*, 116, 20806. [5] M. Futamata, M. Ishikura, C. Iida, and S. Handa, “The critical importance of gap modes in surface enhanced Raman scattering”, *Faraday Discuss.* 2015, 178, 203-220. [6] K. Akai, C. Iida, M. Futamata, “Gap mode Raman spectroscopy under attenuated total reflection geometry”, *J. Opt.* 2015, 11, 114008. [7] C. Iida, K. Akai, J. Murakami, M. Futamata, “Gap mode induced laser trapping of silver nanoparticles on thiophenol-covered silver substrates”, *Chem. Phys. Lett.* 2016, 661, 234-239. [8] M. Futamata, K. Akai, C. Iida, N. Akiba, “Versatile gap mode plasmon under ATR geometry towards single molecule Raman, laser trapping and photocatalytic reactions”, *Anal. Sci.* 2017, 33, 417-426 (Hot article). [9] K. Akai, C. Iida, M. Futamata, “Gap mode induced photocatalytic oxidation of p-alkyl thiophenol molecules on silver films”, *Chem. Phys. Lett.* 2017, 675, 63-68. [10] R. Kuwana, S. Handa, M. Futamata, “Elucidation of hydrated metal ions using flocculation-surface enhanced Raman scattering”, *Chem. Phys. Lett.* 2018, 693, 79-83. [11] S. Nakae, K. Miyashita, M. Futamata, in preparation.

O3-2

High-performance bioelectrocatalysts by immobilization of enzyme onto carbon-coated mesoporous silica membrane.

Tetsuji Itoh,*[ab], Akira Yamaguchi, [c] Yasuto Hoshikawa, [d] Taka-aki Hanaoka [a], Takashi Kyotani[d] and Galen D. Stucky[b]

[a]*National Institute of Advanced Industrial Science Technology (AIST), 4-2-1 Nigatake, Miyagino, Sendai, 983-8551, Japan.*
[b]*Department of Chemistry & Biochemistry, University of California, Santa Barbara, CA 93106-9510, USA.*
[c] *Institute of Quantum Beam Science, Ibaraki University, 2-1-1 Bunkyo, Mito, Ibaraki 310-8512, Japan..*
[d] *Institute of Multidisciplinary Research for Advanced Materials, Tohoku University, 2-1-1 Katahira, Aoba, Sendai, 980-8577, Japan.*
Tel: +81-22-237-3097, Fax: +81-22-237-7027
E-mail:T-Itoh@ni.aist.go.jp

For vital biological functions to occur, the components that make up organs must be arranged appropriately on a nano scale and assume particular higher-order structures. From this perspective, mesoporous materials, which have honeycomb (hexagonal) structures with ordered cylindrical channels 2–10 nm in diameter—larger than the microporous cavities of conventional zeolites (0.6–1.2 nm)—are thought to have potential as capsules for the arrangement of bio-components. Previous efforts to incorporate enzymes that act on comparatively large substrates have been disappointing because substrates have failed to gain entry to the pore structures of mesoporous materials or otherwise remain out of reach of incorporated enzymes. We have successfully encapsulated the monomeric- and subunit-proteins in mesoporous silica or composite membrane with mesoporous silica nanotubes, and in the process, discovered that encapsulation brings about new capabilities[1, 2]. Also, we tried the synthesis of nanoporous silicas in anodic alumina pores, and reported the resultant composite membranes have high potential as artificial membrane supports, owing to a large number of interconnected pores [3] and successfully achieved high sensitive prototype sensor with good stability by encapsulation of enzyme into pores of those membrane [2, 4]. Notably, incorporation appears to increase the stability of the incorporated molecules, creating a platform for host-guest reactions that should support the accumulation and appropriate positioning of enzymes. Here, if mesoporous silicas can be coated with an extremely thin carbon layer, such as a single graphene sheet, the resulting mesoporous silicas, whose ordered mesopore structures remain almost intact, would acquire not only adsorption ability, which contributes to stability, but also electrical conductivity owing to the direct electron transfer between enzymes and the electrode.

In this study, we report the improved applicability of composite membranes containing a mesoporous silica nanotube (F127MST) surface with a coating of an extremely thin carbon layer, comprising only 1–2 graphene sheets, prepared using the chemical vapor deposition (CVD) method. Carbon-coated mesoporous silicas not only offer the advantage of a nano-tailored structure with high adsorption ability, they also can contribute to electrical conductivity, as well as high thermal and chemical stability. And our goal was to achieve direct electron transfer between enzymes and electrodes through establishment of a regular enzyme array by encapsulating it in a carbon-coated composite membrane with mesoporous silica nanotubes. Thus, the system described in this study, in which a bioelectrocatalyst was created through immobilization of an enzyme, represents a viable approach for developing practical and high-performance biofuel cells and biosensors.

[1]Itoh T., Ishii R., Matsuura S., Mizuguchi J., Hamakawa S., Hanaoka T., Tsunoda T., Mizukami F. "Enhancement in thermal stability and resistance to denaturants of lipase encapsulated in mesoporous silica with alkyltrimethylammonium (CTAB)", Colloid Surf. B-Biointerfaces, vol. 75, pp. 478-482, 2010.
[2]Shimomura T., Itoh T., Sumiya T., Mizukami F., Ono M. Electrochemical biosensor for the detection of formaldehyde based on enzyme immobilization in mesoporous silica materials, Sens. Actuat. B: Chem., 135, 268-275, 2008.
[3]Itoh T., Shimomura T., Hasegawa Y., Mizuguchi J., Hanaoka T., Hayashi A., Yamaguchi A., Teramae N., Ono M., Mizukami F. "Assembly of an Artificial Biomembrane by Encapsulation of an Enzyme, formaldehyde dehydrogenase, into the Nanoporous-Walled Silica Nanotube-Inorganic Composite Membrane", J. Mater. Chem., vol. 21, pp. 251-256, 2011.
[4] Itoh T., Shimomura T., Hayashi A., Yamaguchi A., Teramae N., Ono M., Tsunoda T., Mizukami F., Stucky G.D., Hanaoka T. "Electrochemical enzymatic biosensor with long-term stability by using hybrid mesoporous membrane", Analyst, vol. 139, pp. 4654-4660, 2014.

O3-3

A Novel Efficient Antibacterial Action of ABC semiconductors

Kengo Ito[1)], Tohru Nishibe[1)], Masakazu Kawahara[1)], Seiichiro Tsujitsuka[2)], and Kenji Tanaka[2)]

1) Ito Research Institute Co., Ltd.,
2) Department of Biological and Environmental Chemistry, Kindai University
7-1, Shin-Kawasaki, Saiwai-ku, Kawasaki City, Kanagawa, 212-0032 Japan,
Tel: + 81 - 44 - 580-1430, E-mail:kengo.ito@ito-research-institute.co.jp

Introduction

Silver is well known for antibacterial action and has widely been utilized in various applications. Its antibacterial activity is caused by Ag ions which enter the bacteria cells, block metabolism and kill them. Ag ions are not severely hazardous for human bodies and their environment, but it's not that Ag ions are completely safe. In order to exert antibacterial activity for food, Ag bare material should not be touched directly on food and its antibacterial activity keeps only for a short time. We are aiming a novel scheme of antibacterial activity using Ag complex materials, which we call ABC materials[1,2]. Surface plasmon resonance on Ag illuminated by light with specific wavelength induce electrons around ABC and their charges are expected to kill bacteria cells by sort of electromagnetic force. So, indirect antibacterial activity can be observed. In this paper, several results of antibacterial or anti-virus activity will be presented and a possible model for indirect antibacterial activity will be proposed taking account of some suggestive results of ABC semiconductor solar cells[2].

ABC semiconductors

As is shown in Fig.1, ABC semiconductor means the desirable composite of Ag nanoplates, boron, and clay. Plasmon resonance is controlled around Ag plate surface by adjusting its size, and the plasmon energy can be transferred to boron semiconductor and excite it[3]. Boron is incorporated into ABC from the ionic solution including organic compounds of boron and quaternary ammonium cations. It can show both plasmonic and electric properties and is designed so that it is easily printed with appropriate binder. Moreover this material has passed authorized elution tests and safety tests against such as oral poison and fish toxicity. ABC semiconductor will pave the way for various applications other than non-contact antibacterial activity, such as energy harvesting cells with storage effects, functional films that reflect or absorb only the light with specific wavelength up to infrared region, as well as SERS.

Experimental results

First, antibacterial activity to *Escherichia coli* JCM 1649^{T} has been investigated for ABC or AC without B(boron) substrates covered with vitreous coating agent. As is shown in Fig.2, it has been found that indirect antibacterial activity is surely clarified and Ag along with boron plays an important role for this action. Figure 3 shows antibacterial activity of another sample with high concentration ABC covered with urethane resin for *Staphylococcus aureus* NBRC12732. Great antibacterial activity is observed equally both in the dark and under white light illumination. Ag should be excited by light illumination, which will enhance antibacterial activity. Since Ag is very sensitive to feel even slight light, it seems that the difference between dark and illumination is not so clearly observed. But photo-enhanced effects has been observed when the sample is completely shut in the dark before experiment.

Discussion

The principle of photo-voltaic cell completely different from conventional solar cells can partly be tips for our antibacterial action. Figure4 shows a general outline of previous experiments.with the structure of the photo-voltaic cell with ABC and BC,used as a contact electrode, inserted by two ITO electrodes. When light illuminates onto the cell, free electrons oscillate collectively at the surface of Ag plates, induce charge accumulation like a capacitor. Three different compositions of ABC were applied. The result shows photo-voltage generation and relaxation when light is on and off, and ABC composition dependence of rise time and generated photo-voltages, which shows that the plasmon resonance surely induces charge accumulation. It's amazing that fall time reaches up to well over 1 hour. It's negative for fast response devices but it may be desirable for keeping antibacterial activity for a long time.

If we connect above mentioned results with non-contact antibacterial action, a model of array of ABC solar cells in the structure as shown in Fig 5 can be proposed. Illuminated light would cause Ag surface plasmon resonance and collectively oscillating electrons could induce some charge around Ag complex materials, mainly like boron semiconductor, and the charges should form electromagnetic force and kill bacteria. High concentration would make chain like Ag plates, which can generate greater magnetic force.

Future vision

We are now under feasibility study about our novel antibacterial action probably by electron charges against wide range of bacteria and viruses including so called tough ones. Some positive results are obtained. In future, our non-contact antibacterial application will have extensive chances for various kinds of use.

References

[1] K. Ito, Material Forum, Optical Molecule Engineering, sponsored by AIST, Aug. 30 (2013).

[2] T. Nishibe and K. Ito, ",Value-Added ABC Semiconductor Material for Various Applications" Proc. 78th JJSAP-OSA Joint Symposia, Hakata, Japan, 6a-A410-8,Sept. 2017.

[3] Y. Ohko, T. Tatsuma, et.al., “Multicolour photochromism of TiO2 films loaded with silver nanoparticles,” Nature Mater., vol.2, pp.29-31, 2003

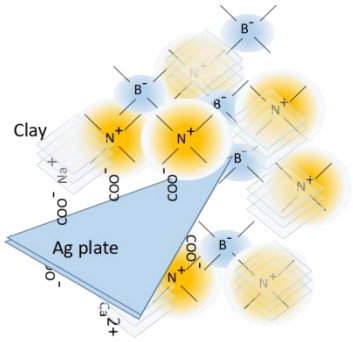

Fig. 1 Schematic diagram of ABC semiconductor

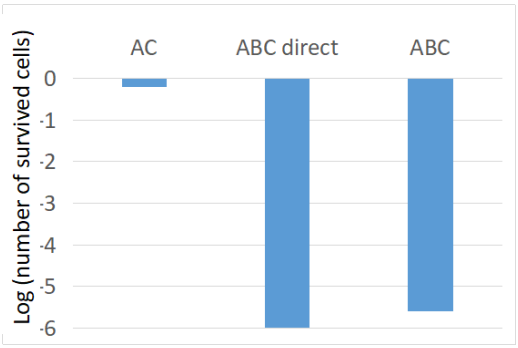

Fig. 2 Non-contact antibacterial activity *to E coli.* Direct experiment showed below -6.

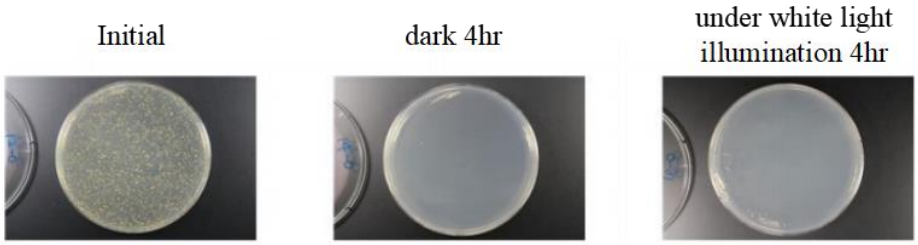

Fig. 3 Non-contact antibacterial activity to *Staphylococcus aureus* NBRC12732 for high concentration ABC covered with urethane film.

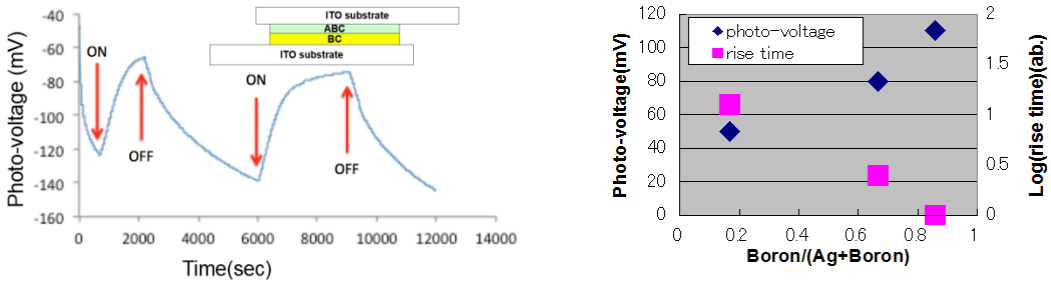

Fig. 4 Photo voltage reaction with light (inset:structure of the solar cell)(left) and photo-voltage and rise tame dependence on AB composition (right)

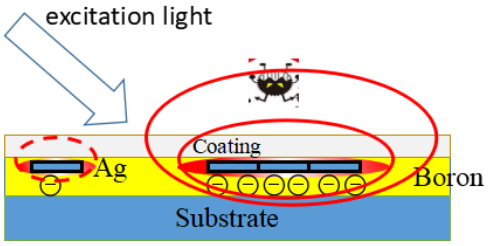

Fig. 5 Possible model of non-contact antibacterial action

O3-4

Observation and Classification of Microorganisms Using Multi-Modal Surface-Enhanced Raman Microscopy Based on Plasmonic Sensors

Morten Bertz[1], Masahiro Yanagisawa[1], Masahiro Kunimoto[1], and Takayuki Homma[1,2]

[1]Research Organization for Nano & Life Innovation, Waseda University
513 Wasedatsurumakicho, Shinjuku-ku, Tokyo, 162-0041, Japan
[2]Dept. of Applied Chemistry, Waseda University
3-4-1, Okubo, Shinjuku-ku Tokyo, 169-8555, Japan
Tel: + 81 - 3 - 5286 - 3209
E-mail: morten.bertz@aoni.waseda.jp

In recent years, surface-enhanced Raman scattering (SERS) has emerged as a powerful technique that permits highly sensitive detection of low concentration analytes. Leveraging the amplification of electrical fields by generation of localized surface plasmons, SERS allows for facile, non-destructive, label-free, rapid, and relatively inexpensive analysis of a wide variety of samples. Here, we discuss our recent progress combining plasmonic nanosensors combined with confocal microscopy to detect, classify, and observe micron-sized biological or organic samples in real time.

Employing substrates coated with nanoparticles of plasmon-active metals (Au or Ag), we attempt to identify various microbial air contaminants, such as spores, bacteria, and fungi, by their vibrational signature. Microbial samples placed on these surfaces require no labelling prior to analysis, and a characteristic spectral signature for a single cell can be obtained within seconds at low incident laser power. As plasmonic enhancement occurs at the metal nanoparticle surface, cellular constituents within 10-20 nm to the substrate have the strongest contribution to the observed Raman signal. The surface of microorganisms is a heterogeneous structure, and we can therefore observe spectral fluctuations even within the same sample at high temporal and spatial resolution. The temporal fluctuations likely stem from micro- and macroscopic sample movements, and the relative Raman band intensities reflect the cell surface components in contact with the plasmonic sensor at a given point in time. Despite considerable variation among individual spectra, mixtures of 4 different samples can be can be classified beyond 85 % confidence using a machine-learning approach.

In addition, we combine confocal Raman microscopy with video imaging and surface topography mapping based on light scattering. The short data acquisition times enabled by SERS allow surfaces to be mapped essentially at video rate. Imaging and topography data can in principle be used to facilitate sample location and provides additional information about sample type and morphology. Furthermore, each Raman spectrum can be correlated unambiguously with a location on the sample cell. We anticipate that employing such a multi-modal approach will be an important factor in developing fully autonomous systems for detection, observation, and classification.

Acknowledgements
The authors gratefully acknowledge support by the project “Development of Systems and Technology for Advanced Measurement and Analysis”, Japan Science and Technology Agency.

O3-5

Spatially-defined electroless copper plating on microstructured PDMS surfaces

T. Sato[1], C. Urata[1], N. Singh[1], A. Manettas[1], Y. Matsuo[2] and A. Hozumi[1]*

[1]*National Institute of Advanced Industrial Science and Technology (AIST)*
2266-98, Anagahora, Shimoshidami, Nagoya 463-8560, Japan
Tel: + 81 - 52 - 736 - 7388, Fax: + 81 - 52 - 736 - 7406
E-mail: a.hozumi@aist.go.jp
[2]*Research Institute for Electronic Science, Hokkaido University*

Introduction

Metallization on polymer substrates, such as resins and rubbers, has attracted much attention lately. In particular, electroless plating on microstructured polymer surfaces is becoming an important technology for the fabrication of microelectronic devices [1]. To realize spatially-defined electroless plating on the microstructured polymer surfaces with reasonable thickness, and adhesion of the metal layers, pre-treatments of the polymer surfaces are of crucial importance, because metallization proceeds preferentially in the specifically-defined regions covered with the plating catalyst.

Methods

In this study, three different types of pre-treatments were demonstrated on the poly(dimethylsiloxane) (PDMS) surfaces with and without microstructures to anchor Pd catalysts for electroless copper (Cu) plating.

Briefly, 1) 3-aminopropyltriethoxysilane (APTES) monolayer, 2) polydopamine (PDA) multilayer [2], and 3) poly[2-(dimethylamino)ethyl methacrylate] (PDMAEMA) polymer brush [3] were first prepared on the PDMS surfaces by CVD, electrochemical deposition, and surface initiated (SI)-"Paint-on" atom transfer radical polymerization (ATRP), respectively. After immobilization of Pd catalyst, electroless Cu plating was finally demonstrated on these substrates for a certain time.

Results and Discussion

We first observed surface morphologies of the resulting Cu layers formed on the flat PDMS surfaces by optical microscope and scanning electron microscope (SEM). A homogeneous Cu layer was successfully deposited on every sample surfaces macroscopically and microscopically (Figure 1). However, the growth rate of the Cu layer on the PDMAEMA-modified PDMS surface (41 nm/min) was much higher than those on the other APTES- and PDA-modified PDMS surfaces (27 and 24 nm/min, respectively). This suggests that brush structures of PDMAEMA layer effectively worked to immobilize sufficient amount of the Pd catalyst, resulting in the high growth rate. In addition, the Cu layer formed on the PDMAEMA-modified surface was firmly adhered to the PDMS surface, and did not peel off even after bending and a simple tape peeling tests. Based on the optimum conditions, we have also successfully demonstrated spatially-defined electroless plating on the microstructured PDMS surfaces (Figure 2).

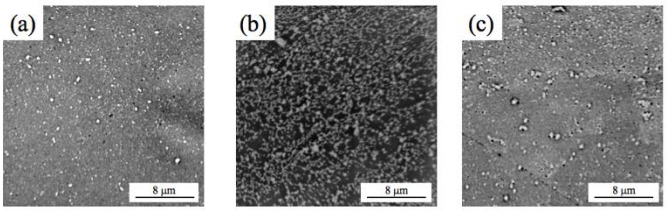

Figure 1. SEM images of Cu layers deposited on (a) APTES-, (b) PDA-, (c) PDMAEMA- modified PDMS.

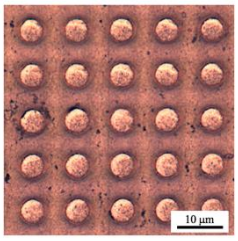

Figure 2. Typical optical microscope image of microstructured Cu/PDMS (PDMAEMA modified) surface.

Judging from these results, we conclude that formation of the polymer brush by SI-"Paint-on" ATRP [3] is one of the most effective pre-treatment methods for the metallization of PDMS substrates. This method is not limited to only polymer substrates, but is applicable to various substrates.

References

[1] O. Azzaroni, Z. Zheng, Z. Yang, and W. T. S. Huck, "Polyelectrolyte brushes as efficient ultrathin platforms for site-selective copper electroless deposition", Langmuir, vol.22, no.16, pp.6730-6733, June 2006.

[2] H. Lee, W. Dellatore, M. Miller, and P. B. Messersmith, "Mussel-inspired surface chemistry for multifunctional coatings" Science, vol.318, no. 5849, pp.426-430, October 2007.

[3] G. J. Dundardale, C. Urata, D. F. Miranda and A. Hozumi, "Large-scale and environmentally friendly synthesis of pH-responsive oil-repellent polymer brush surfaces under ambient conditions" ACS Appl. Mater. Interfaces, vol.6, no.15, pp.11864-11868, July 2014.

O3-6

Structural and Photoluminescence Properties of ZnO Nanorods Grown by Chemical Bath Deposition and Formation of PEDOT:PSS/ZnO Nanorods Heterojunctions

Tomoaki Terasako [1], Shohei Obara [1] Masakazu Yagi [2], Junichi Nomoto [3] and Tetsuya Yamamoto [3]

[1] Graduate School of Science and Engineering, Ehime University,
3 Bunkyo-cho, Matsuyama, Ehime, 790-8577 Japan
Tel: + 81 - 89 - 927 - 9789, Fax: +81- 89 -927 – 9790
E-mail:terasako.tomoaki.mz@ehime-u.ac.jp
[2] National Institute of Technology, Kagawa College
551 Koda, Takuma-cho, Mitoyo, Kagawa, 769-1192, Japan
[3] Materials Design Center, Research Institute, Kochi University of Technology
185 Miyanokuchi, Tosayamada-cho, Kami, Kochi, 782-8502, Japan

Zinc oxide (ZnO) with a direct band gap of ~3.37 eV at RT and a large exciton binding energy of ~60 meV is one of the promising materials for optoelectronics devices, solar cells, spintronics devices, sensing devices and so on [1]. For the surface utilization devices, such as semiconductor electrodes for dye-sensitized solar cells, gas-, chemical- and bio-sensors, it is expected that the increase in specific surface area introduced by forming nanostructures contributes to the improvement of the device performance [2]. Nanostructures of ZnO have been successfully grown by various growth techniques so far. Among the various growth techniques, we have paid our attention to chemical bath deposition (CBD) because this technique is usually performed at low temperatures (<100 °C), which allows us to use polymers as substrate materials. We have reported the successful growth of ZnO nanorods (NRs) on the Au/SiO_2/Si(100) substrates by CBD using different Zn precursors, *i.e.* $ZnCl_2$, $Zn(CH_3COO)\cdot 2H_2O$ and $Zn(NO_3)_2\cdot 6H_2O$ (ZnNit) [3,4]. In this paper, the possibility of morphology-controlled CBD growth of ZnO NRs on the Au and ZnO:Ga (GZO) seed layers, and effects of the difference in seed layer on their structural and photoluminescence (PL) properties will be discussed. Moreover, fabrication of the heterojunctions of ZnO NRs with PEDOT:PSS layer will be attempted.

The substrate materials used in this study were (1) Au/SiO_2/Si(100) wafers, (2) commercial Au/Ti/Si(100) wafers and (3) ion-plated 200 nm GZO/glass films [5]. Mixed aqueous solutions of ZnNit and $C_6H_{12}N_4$ (HMT) were used as the CBD solution. The molar ratio of ZnNit to HMT in the CBD solution was kept at 1:1. The reaction was carried out at ~88 °C. Growth time (t_g) was varied in the range from 5 to 360 min.

All the X-ray diffraction (XRD) patterns of the samples grown on the GZO and Au seed layers were dominated by the (002) peak, indicating the preferential *c*-axis growth. Scanning electron microscope (SEM) observations revealed that all the NRs on the GZO/glass substrates were aligned perpendicular to the substrate surface, whereas some of the NRs grown on the Au/SiO_2/Si(100) and Au/Ti/Si(100) substrates were inclined from the direction perpendicular to the substrate surface. The growth time dependences of the average width and average length for the ZnO NRs grown on the different seed layers are shown in Fig. 1. For all the seed layers, within t_g=60 min, the average width and average length of the NRs increase rapidly with t_g. Above t_g=60 min, the average widths of the NRs grown on the GZO/glass, Au/SiO_2/Si(100) and Au/Ti/Si(100) substrates were saturated at ~200 nm, ~400 nm and ~1000 nm, respectively. In contrast to the average width, no remarkable difference can be seen among the growth time dependences of the average length of the NRs grown on the different seed layers. The XRD measurements for the seed layers imply that the saturated value of the average width has some connection with the average grain size of the seed layer.

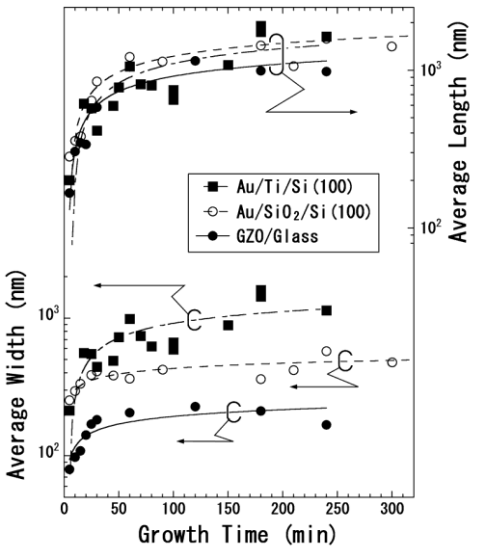

Fig. 1 Variations of average width and average length as a function of growth time (●: ZnO NRs/GZO/glass, ○: ZnO NRs/Au/SiO_2/ Si(100), ■: ZnO NRs/Au/Ti/Si(100))

Fig 2 shows PL, photoluminescence excitation (PLE) and photoacoustic (PA) spectra of the NRs grown on the GZO/glass films for the different t_gs. Regardless of the difference in seed layer, all the PL spectra were composed of a near band-edge (NBE) emission at ~380 nm and an orange band (OB) emission at ~630 nm. So far many researchers have reported that the OB emission is related to oxygen interstitial defects (O_is) [6-8]. Therefore, the appearance of the OB emission suggests that the ZnO NRs grown

by CBD are in oxygen rich compositions. Moreover, it was found that, for the ZnO NRs grown on the GZO/glass and Au/SiO_2/Si(100) films, the PL intensity ratio of the NBE emission to the OB emission became larger with t_g, indicating the improvement of the crystalline quality. For the ZnO NRs grown on the Au/Ti/SiO_2/Si(100) films, however, the NBE emission was negligible weak over all t_gs. For the NRs grown on the GZO/glass films for t_g=60-240 min, interestingly, the OB emission is effectively excited through the formation of the excitons as shown in Fig. 2.

The PEDOT:PSS (Sigma-Aldrich, 1.0 wt.% in H_2O, High conductivity grade) layers were spin-coated on the surfaces of the ZnO NRs/GZO/glass and GZO/glass films at 1500-2000 rpm for 5-10 sec followed by the thermal annealing in the atmosphere at 120-150 °C for 60 min. Fig. 3 shows the voltage-current curves of the PEDOT:PSS/GZO and PEDOT:PSS/ZnO NRs/GZO heterojunctions. For the PEDOT:PSS/GZO heterojunction, the absolute value of the forward current is almost equivalent to that of the backward current. The voltage-current curve of the PEDOT:PSS/GZO heterojunction changes dramatically by inserting the ZnO NRs layer. As a result, the voltage-current curve of the PEDOT:PSS/ZnO NRs/GZO heterojunction exhibits a rectifying characteristic. However, further growth experiments of the PEDOT:PSS layers under the different spin-coating and post annealing conditions are required for obtaining favorable voltage-current characteristics.

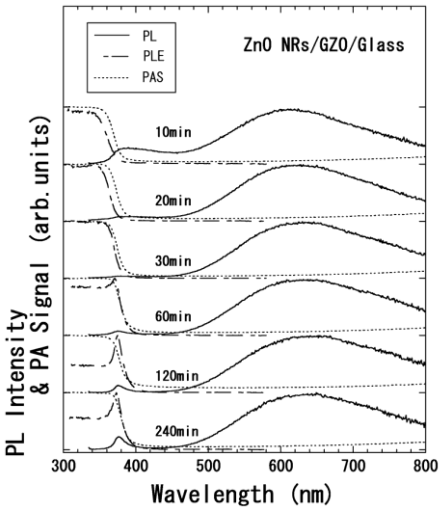

Fig. 2 PL (solid line), PLE (alternate long and short dash line) and PA (dotted line) spectra of the ZnO NRs/GZO/glass films grown for the different growth times.

This work was supported by JSPS KAKENHI Grant Number JP17K04989 and Yashima Environment Technology Foundation.

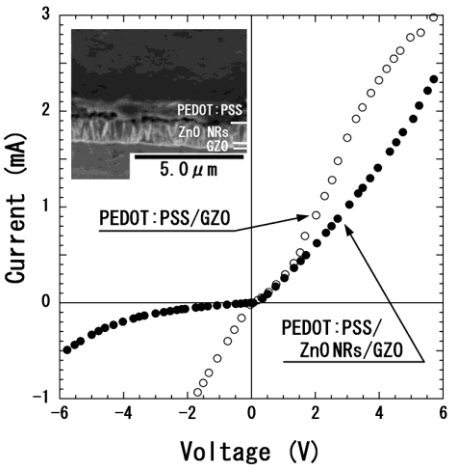

Fig. 3 Voltage-current curves of PEDOT: PSS/GZO and PEDOT:PSS/ZnO NRs/ GZO heterojunctions. The inset shows the bird's view SEM image of the PEDOT: PSS/ZnO NRs/GZO heterojunction.

References

[1] C. Jagardish, S. Pearton ed. Zinc Oxide Bulk, Thin Films and Nanostructures, Processing, Properties and Applications, Elsevier, Amsterdam, 2006.

[2] E. Comini, G. Sberveglieri, "Metal oxide nanowires as chemical sensors," Mater. Today, vol.13, Issue 7-8, pp.36-44, 2010.

[3] T. Terasako, T. Murakami, M. Yagi, S. Shirakata, "Shape Controllability and photoluminescence properties of ZnO nanorods grown by chemical bath deposition," Thin Solid Films, vol.549, pp292-298, December 2013.

[4] T. Terasako, T. Murakami, A. Hyodou, S. Shirakata, "Structural and electrical properties of CuO films and *n*-ZnO/*p*-CuO heterojunctions prepared by chemical bath deposition based technique," Sol. Energy Mater. Sol. Cells, vol.132, pp.74-79, January 2015.

[5] J. Nomoto, H. Makino, T. Yamamoto, "Limiting factors of carrier concentration and transport of polycrystalline Ga-doped ZnO films deposited by ion plating with dc arc discharge," Thin Solid Films, vol.601, pp.13-17, February 2016.

[6] S. A. Studenikin, N. Golego, M. Concivera, "Fabrication of green and orange photoluminescent, undoped ZnO films using spray pyrolysis," J. Appl. Phys. vol.84, Issue 4, pp.2287-2294, August 1998.

[7] H. Fan, S. Yang, P. Zhang, H. Wei, X. Liu, C. Jian, Q. Zhu, Y. Chen, Z. Wang, "Investigation of oxygen vacancy and interstitial oxygen defects in ZnO films by photoluminescence and x-ray photoelectron spectroscopy," Chin. Phys. Lett. vol.24, Issue 7, pp.2108-2111, July 2007.

[8] D.C. Halls, C. Leach, "Spectroscopic cathodoluminescence studies of additive free zinc oxide and varistor ceramics," Acta Mater. vol.46, Issue 17, pp.6237-6243, November 1998.

O3-7

AuGe source and drain formation for the scaling of bottom-contact type pentacene-based OFETs

Shun-ichiro Ohmi, Mizuha Hiroki, and Yasutaka Maeda

Electrical and Electronic Engineering, Tokyo Institute of Technology,
J2-72, 4259 Nagatsuta, Midori-ku, Yokohama 226-8502, Japan
Phone&Fax: + 81 - 45 - 924 – 5481
E-mail: ohmi@ee.e.titech.ac.jp

Abstract

The organic field-effect transistors (OFET) with bottom-contact (BC) source and drain (S/D) geometry are suitable for the device scaling and integration. Au is usually used for the S/D electrodes in p-type OFETs. However, Au has an issue to form BC S/D such as the adhesion problem on SiO_2. In this paper, we investigated the AuGe-alloy S/D for the BC S/D [1]. The AuGe is a popular material as the contact electrodes for the compound semiconductor devices.

Figure 1 shows a plane-view and the schematic cross-section of the fabricated back-gate (BG) type BC S/D pentacene-based OFET [1]. The 10 nm-thick SiO_2 was formed on n^+-Si(100) substrate. Then, the 40 nm-thick AuGe was deposited by thermal evaporation, and the BC S/D was patterned by the lift-off process using OFPR as a resist. The Ge composition was changed from 0% (Au) to 7.4% (Au-7.4%Ge). Then, a 10 nm-thick pentacene film was deposited by thermal evaporation at room temperature (RT) without patterning. The channel length (L) and width (W) were 2.4 - 20 and 160 μm, respectively. Figure 2 shows the plane-views of the fabricated BG/BC-OEFTs. The minimum channel length of 2.4 - 2.5 μm was successfully fabricated as shown in Fig. 2. However, the fabrication yield of Au S/D was 57% shown in Fig. 2(a). The yield was found to be increased to 93% for Au-1%Ge S/D (Fig. 2(b)) and 100% for Au-7.4%Ge S/D (Fig. 2(c)). This is probably because the improvement of the adhesion ability to SiO_2 by incorporation of Ge in Au. Figure 3 shows the channel length dependence of the extracted mobility (μ) at the operation voltage of V_D = - 5 V. The mobility of the Au-7.4%Ge S/D OFET with L/W=2.4/160 μm was 1.1×10^{-3} $cm^2/(Vs)$, while it was 5.7×10^{-3} $cm^2/(Vs)$ for the Au S/D OFET with L/W=2.4/160 μm. Interestingly, the mobility for Au-1%Ge S/D shows severe degradation than that of Au-7.4% S/D OFET. This is probably caused by the contact issues between the pentacene and AuGe S/D depending on the Ge compositions. Although the mobility was decreased compared with the Au S/D OFET, it would be improved by optimization of the surface treatment process after the BC S/D formation.

In summary, the fabrication yield of BC OFET was significantly improved by using the Au-7.4%Ge S/D, and it is a promising material for the future scaling of BC OFETs.

Acknowledgements

This research was partially supported by JSPS KAKENHI Grant Number 15K13969.

References

[1] M. Hiroki, Y. Maeda, and S. Ohmi, "Top-gate pentacene-based organic field-effect transistor with amorphous rubrene gate insulator", Jpn. J. Appl. Phys., **57**, 02CA08 (2018).

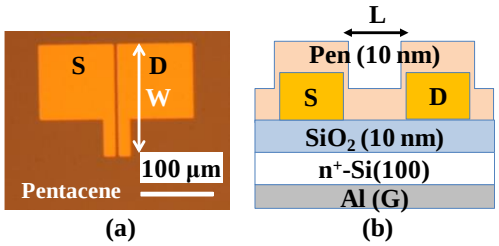

Fig. 1 (a) Plane-view and (b) schematic cross-section of fabricated BG/BC pentacene-based OFET.

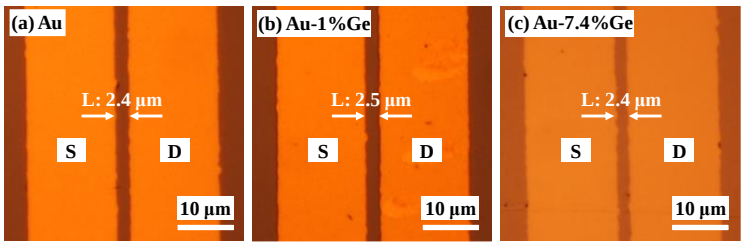

Fig. 2 Plane-views of the fabricated BG/BC pentacene-based OFETs with S/D of (a) Au, (b) Au-1%Ge, and (c) Au-7.4%Ge. The L/W was 2.4-2.5/160 μm.

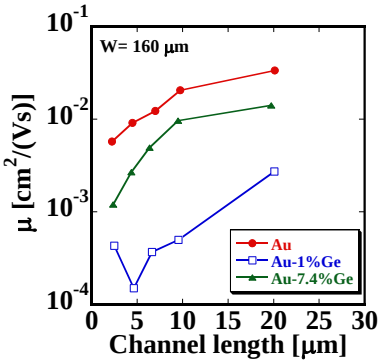

Fig. 3 Channel length dependence of the mobility for the fabricated BG/BC pentacene-based OFETs.

O3-8

Single crystallization of thienoacene-based semiconductors in gel capillaries

Satoshi Watanabe 1,2 Ryota Urata 1 and Masashi Kunitake 1,2

[1]Department of Applied Chemistry and Biochemistry, Kumamoto University,
2-39-1 Kurokami, chuou-ku, kumamoto city, Kumamoto, 860-8555, Japan.
[2]Coordination Asymmetry, Grant-in-Aid for Scientific Research on Innovative Areas
Tel: +81-96-342-3674
E-mail:watasato@kumamoto-u.ac.jp

Single crystals of organic semiconductors have attracted much attention because of the good carrier mobility on field effect transistors. Patterning technique of single crystals have been studied for application to integrated organic field effect transistors. Some printing techniques succeeded in patterning the single crystals using concentration gradient in the inks[1, 2]. However, size down or alignment of the single crystals is difficult due to the diffusion of the concentration gradient which caused the difficulty on keeping crystal growth conditions constant. We have studied quasi phase diagrams at each interface for the liquid phase crystallization which can easily control the crystallization conditions by adjusting temperature.[3] In this study, we fabricated the single crystals of thienoacene derivatives in gel capillaries for making rod plate shape of the single crystals and transferring them to solid substrates.

2, 7-Dioctyl [1] benzothieno [3, 2-b] [1] benzothiophene (C8-BTBT) were dissolved in o-dichlorobenzene (ca. 100 mM) and filled in capillaries of agarose hydrogels at a dimeter of ca. 500 μm. The one side of the solutions is in air and the other is water. Samples were cooled down at 1 °C per 5 min each until temperature reached at the nucleation temperature (13 °C) of the air/liquid interfaces. After selective nucleation at the air/liquid interfaces, the temperature kept the constant for 24-48 h for growth of the crystals. The solution was replaced with pure water. The gel samples were immersed in NaI solutions to dissolve the gels, resulting in the single crystals floated on the water solution. The crystals were transferred from the hydrophilic surface of Si wafers by putting the substrates onto the water. The samples were observed by crossed Nicol microscopy.

Above 13 °C, the crystals were not observed in any places of the capillaries. After cooling down at 13 °C, the crystals were formed selectively at the air/liquid interfaces within 5 min. Without interface, the nucleation did not occurs in the bulk solutions at this temperature. This is due to the Gibbs adsorption of C8-BTBT at the air/liquid interfaces, leading to an increase of the concentration at the interfaces. These crystals grew from the interface to the center of bulk solutions. After grown sub millimeters from the interfaces, only one crystal can be seen. The crystal remained unchanged after the replacement of the ink solutions with waters. The dissolution of the gels leads to the crystals floated on the NaI solutions. The hydrophobic Si substrates can easily catch the crystals from the water surfaces. Figure 1a shows the crossed Nicol image of the crystal transferred on the Si substrates. The width and length of the crystals is about 0.5 mm and 2.3 mm, respectively. The poly crystals at the left side of the crystal were not transferred from the water at this time. Some aggregates were formed on the edge and surface of the crystal during the transferring step. A rotation of the sample at 45 ° against long axis of the crystal disappear the crystal image, indicating that this crystal without the aggregates is a single crystal.

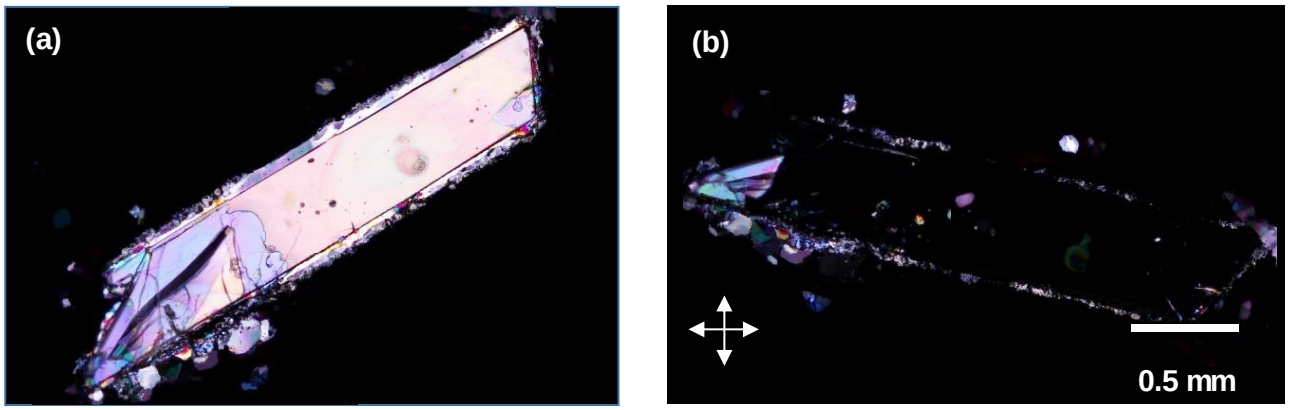

Figure 1. Crossed-Nicol image of a C8-BTBT single crystal fabricated in gel capillaries and transferred on Si substrates at (a) reference axis, (b) 45 °.

[1] T. Hasegawa et al., “Inkjet printing of single-crystal films” Nature, vol.475, pp. 364−367, 2011.
[2] Z. Bao et al., “High-mobility, aligned crystalline domains of TIPS pentacene with metastable polymorphs through lateral confinement of crystal growth” Adv. Mater. vol.26, pp. 487−493, 2014.
[3] S. Watanabe et al., "Quasi-phase diagrams at air/oil interfaces and bulk oil phases for crystallization of small-molecular semiconductors by adjusting Gibbs adsorption" Langmuir, vol.33, pp. 8906−8913, 2017.

O4-1

Development of organic solar cells using MoO_3 / Mg cathode interlayers

Iwamichi Ishikawa, Akira Higa and Hiroshi Kageyama

Department of Electrical and Electronics Engineering, Faculty of Engineering,
University of the Ryukyus,
1 Senbaru, Nishihara, Okinawa 903-0213, Japan
Tel: + 81 - 98 - 895 -8746, Fax: +81 - 98 - 895 -8746
E-mail: kageyama@tec.u-ryukyu.ac.jp

Optimization of the organic photoactive material / electrode interface is crucial for the improvement of organic solar cells (OSCs) performance because OSCs consist of thin films of organic photoactive materials sandwiched between two electrodes. In the present study, we demonstrated that the insertion of MoO_3 / Mg layers between organic photoactive material / cathode interface improves fill factors (FFs), thus improves power conversion efficiencies (PCEs).

To investigate the effect of the MoO_3 / Mg cathode interlayers on OSC performance, OSCs using the cathode of bare Al (Device A), Mg / Al (Device B) and MoO_3 / Mg / Al (Device C) were fabricated and their performance was examined. The structures of Device A~C are shown in Figure 1.

Figure 2 shows current density - voltage (*J*-*V*) characteristics of Device A~C under AM1.5G illumination at an incident light intensity of 100 mWcm^{-2}. Device A using the cathode of bare Al showed a J_{SC}, an open-circuit voltage (V_{OC}), a FF, and a PCE of 9.5 mAcm^{-2}, 0.66 V, 0.29 and 1.8 %, respectively. Device B using the Mg / Al cathode showed higher J_{SC}, V_{OC} and FF (10.6 mAcm^{-2}, 0.92 V and 0.49, respectively), thus showed a higher PCE of 4.7% than Device A. On the other hand, Device C using the MoO_3 / Mg interlayer exhibited higher FF of 0.59 than those observed for Device B, while maintaining almost the same J_{SC} and V_{OC} values (10.5 mAcm^{-2} and 0.92 V, respectively) as those for Device B, thus exhibited the higher PCE of 5.7 % than Device B. These results indicate that the thin films of MoO_3 / Mg function as cathode interlayers which improve FF.

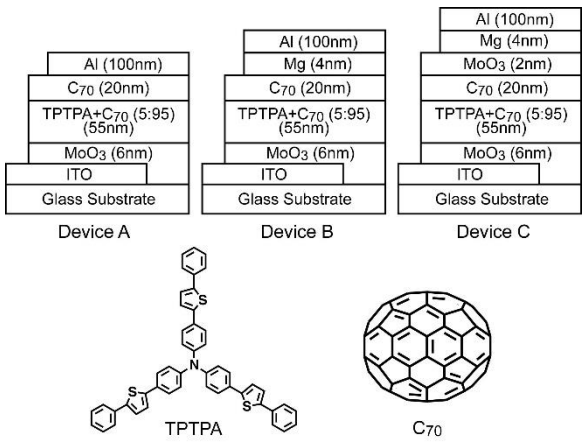

Figure 1 Structures of Device A~C, and molecular structures of TPTPA and C_{70}.

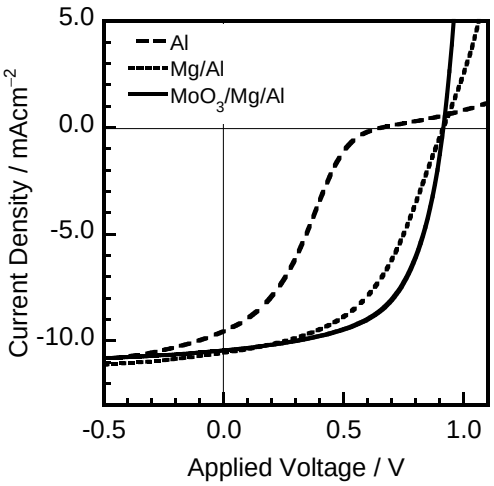

Figure 2 *J*-*V* characteristics of Device A ~ C under illumination of simulated solar light (AM1.5G, 100 mWcm^{-2})

O4-2

Direct imaging of photonic nanojets generated from a self-assembled liquid crystal microdroplet utilizing laser-scanning confocal microscope

Tatsunosuke Matsui, Takeru Nihashi and Kazuya Tsukuda

Department of Electrical and Electronic Engineering, Graduate School of Engineering, Mie University
1577 Kurimamachiya, Tsu, Mie, 514-8507, Japan
Tel: + 81 - 59 - 231 - 9030, Fax: +81- 59 -231 - 9409
E-mail:matsui@elec.mie-u.ac.jp

In recent years, much effort has been devoted to confine the light to a tiny spot beyond the diffraction limit, and novel type of nano-optics has emerged such as near-field optics, plasmonics, and meta-optics. In these nano-optical systems, state-of-the-art micro-fabrication techniques are usually required to fabricate materials and devices.

In 2004, Chen *et al*. discovered the phenomenon called photonic nanojet (PNJ), in which a jet-like light wave with subwavelength beam waist could be obtained with quite simple geometry [1]. They demonstrated based on a finite-difference time-domain (FDTD) numerical simulation that upon illuminating a μm-sized lossless dielectric microcylinder or microsphere with a plane wave light, a propagating light beam that is narrow, bright, and can propagate over a distance longer than the wavelength, could be obtained from the shadow-side surface of the microcylinder or microsphere [1]. PNJ was later directly observed by utilizing a laser-scanning confocal microscope (LSCM) [2]. Various types of applications based on the PNJ have been proposed and demonstrated, such as spectroscopy [1], optical lithography [3-5], super-resolution microscopy [6-9], etc. Here, we show that PNJ can be obtained and dynamically controlled by using a liquid crystal (LC) microdroplet [10].

LC microdroplets can be formed in a self-organizing manner when LC molecules are dispersed in a liquid or polymer matrix. The orientation of LC molecules can be controlled by applying an external electric field. The operation principle of our PNJ generator based on a LC microdroplet is schematically shown in Fig. 1.

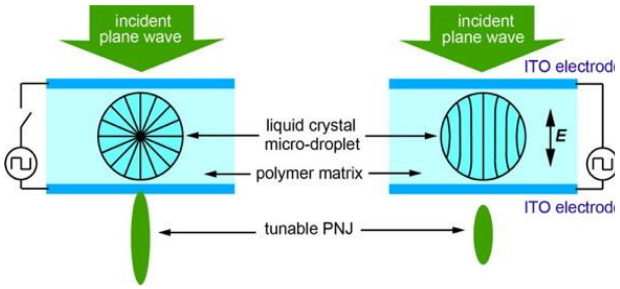

Fig. 1: Schematic of tunable PNJ generator based on a self-assembled LC microdroplet.

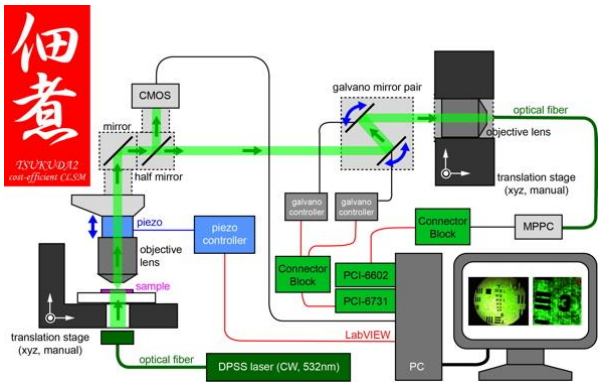

Fig. 2: Schematic of home-built LSCM system TSUKUDA2.

In our study, nematic LC E7 and polydimethylsiloxane (PDMS) are used to fabricate LC microdroplets. The LC microdroplet with a diameter of 5 μm are chosen for the observation of PNJ. Such LC microdroplets were fabricated in between indium-tin-oxide (ITO)-coated glass slides for external voltage application. A home-built LSCM system schematically shown in Fig. 2 was used to observe the obtained PNJ under external voltages. Main framework of our LSCM system is constructed based on a 30 mm cage system of Thorlabs Inc. A diode-pumped solid-state (DPSS) laser operating at 532 nm was used as a light source. The transmitted (scattered) light was collected with an objective lens, which was attached to the piezo actuator designed to finely adjust a focal point along an optical z-axis of the system. A half of the collected light was sent to the CMOS device for optical imaging, and the rest was sent to the pair of two galvanometers for confocal imaging. 3D observation was performed by scanning the laser spot transversely in x-y plane by the galvanometers and horizontally along z-axis by the piezo actuator attached to the objective lens. The

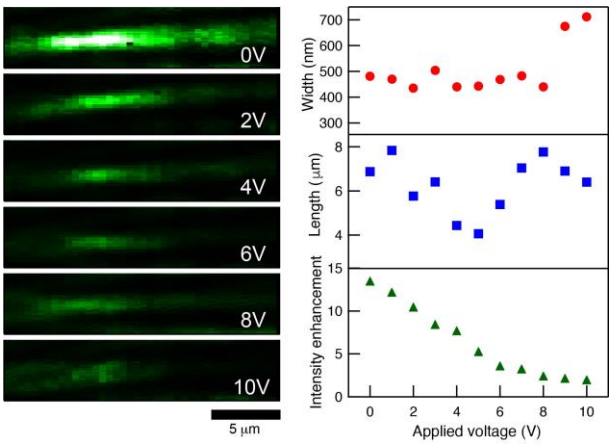

Fig. 3: PNJ generated by a LC microdroplet under applied voltage observed by a home-built LSCM and a summary of beam width, beam length, and intensity enhancement of the PNJ as a function of applied voltage.

light from galvanometers was collected and focused with another objective lens to couple to the multimode optical fiber, which also worked as a pinhole for confocal imaging to reject out-of-plane and out-of-axis light. Multi-pixel photon counter (MPPC) module, which is capable of a photon counting-level detection, was used for detecting light intensity and counter/timer device was used for photocounts acquisition. Scanning of the laser spot and data acquisition were synchronized and controlled in a LabVIEW environment.

PNJs with subwavelength beam waist were successfully obtained from LC microdroplets of 5 μm diameter. By applying external voltage of a few volts some of major properties of PNJs such as beam length and brightness are tuned as summarized in Fig. 3. Electro-tunable PNJs from self-assembled LC microdroplets may be utilized to develop novel type of micro-optical devices such as spectroscopy, optical data storage, optical lithography, super-resolution microscopy, etc.

This study has been partly supported by Grant-in-Aid for Scientific Research, KAKENHI, for Young Scientists (B) (26820111) from Japan Society for the Promotion of Science (JSPS), Toyota Physical and Chemical Research Institute, and Research Foundation for the Electrotechnology of Chubu (REFEC).

References

[1] Z. Chen, A. Taflove, and V. Backman, “Photonic nanojet enhancement of backscattering of light by nanoparticles: a potential novel visible-light ultramicroscopy technique,” Opt. Express, vol.12, no.7, pp.1214-1220, April 2004.
[2] P. Ferrand, J. Wenger, A. Devilez, M. Pianta, B. Stout, N. Bonod, E. Popov, and H. Rigneault, “Direct imaging of photonic nanojets,” Opt. Express, vol.16, no.10, pp.6930-6940, May 2008.
[3] W. Wu, A. Katsnelson, O. G. Memis, and H. Mohseni, “A deep sub-wavelength process for the formation of highly uniform arrays of nanoholes and nanopillars,” Nanotechnology, vol.18, pp.485302-1-4, October 2007.
[4] E, McLeod, and C. B. Arnold, “Subwavelength direct-write nanopatterning using optically trapped microspheres,” Nature Nanotech., vol.3, pp.413-417, July 2008.
[5] J. Kim, K. Cho, I. Kim, W. M. Kim, T. S. Lee, and K.-S. Lee, “Fabrication of Plasmonic Nanodiscs by Photonic Nanojet Lithography,” Appl. Phys. Express, vol.5, no.2, pp.025201-1-3, January 2012.
[6] Z. Wang, W. Guo, L. Li, B. Luk’yanchuk, A. Khan, Z. Liu, Z. Chen, and M. Hong, “Optical virtual imaging at 50 nm lateral resolution with a white-light nanoscope,” Nature Commun., vol.2, pp.218-1-6, March 2011.
[7] A. Darafsheh, G. F. Walsh, L. D. Negro, and V. N. Astratov, “Optical super-resolution by high-index liquid-immersed microspheres,” Appl. Phys. Lett., vol.101, no.14, pp.141128-1-4, October 2012.
[8] K. W. Allen, N. Farahi, Y. Li, N. I. Limberopoulos, D. E. Walker Jr., A. M. Urbas, and V. N. Astratov, “Overcoming the diffraction limit of imaging nanoplasmonic arrays by microspheres and microfibers,” Opt. Express, vol.23, no.19, pp.24484-24496, September 2015.
[9] L. Friedrich, and A. Rohrbach, “Surface imaging beyond the diffraction limit with optically trapped spheres,” Nature Nanotech., vol.10, pp.1064-1069, December 2015.
[10] T. Matsui, and K. Tsukuda, “Direct imaging of tunable photonic nanojets from a self-assembled liquid crystal microdroplet,” Opt. Lett., vol.42, no.22, pp.4663-4666, November 2017.

04-3

Improved characteristics of top-gate-type organic light-emitting transistors based on Super Yellow emissive layers with various annealing temperatures

Hirotake Kajii, Takayuki Mashimo and Masahiko Kondow

Graduate School of Engineering, Osaka University,
2-1 Yamada-oka, Suita, Osaka, 565-0871 Japan
Tel: + 81 - 6 - 6879 -7766, Fax: + 81 - 6 - 6879 - 7766
E-mail:kajii@eei.eng.osaka-u.ac.jp

The internet of Things (IoT) is supported by various sensor and display devices. Microlight sources based on organic light-emitting transistors (OLETs) with an electrical switching capability, in which not only the position and extension of the emission area but also the emission color are controlled by gate voltage(V_G) and drain voltage (V_D), are useful for augmented (AR) and virtual reality (VR) displays and sensor applications.

In organic semiconductors, π-conjugated polymers, being quasi-one-dimensional macromolecular electronic systems, offer a number of unique properties. A poly(*p*-phenylene vinylene) derivative, Super Yellow (SY) is one of the most important class of conjugated polymers due to their efficient emission. Time of flight measurements of charge mobility in SY films showed mobilities in the range 10^{-6} – 10^{-7} $cm^2V^{-1}s^{-1}$ [1].The effect of thermal annealing SY thin films during organic light-emitting diode fabrication has been reported [2]. The characteristics of bottom-gate-type OLET based on SY active layer have been demonstrated. The bottom-gate-type OLETs with Au and Ca source/drain (S/D) electrodes exhibited the ambipolar characteristic with the hole field-effect mobility of 10^{-4} – 10^{-5} $cm^2V^{-1}s^{-1}$ order and the electron field-effect mobility of 10^{-5} $cm^2V^{-1}s^{-1}$ order [3, 4].

For devices with bottom-contact/top-gate geometry, charge injection can be expected to occur a large area away from the edge of electrodes and be aided due to the influence of the applied gate filed. During annealing process, the surface of organic film, where the channel is formed in top-gate-type device, is well self-organized, compared with the bottom of organic film in bottom-gate-type device. In this study, we investigated the improved characteristics of top-gate-type OLETs based on SY active layers with various annealing temperatures.

Film formation is performed by spin coating. Poly(methyl methacrylate) (PMMA), which does not contain electron-trapping groups such as OH, is one of the promising candidate gate dielectrics in OLETs. A silver (Ag) gate electrode was then vacuum-evaporated onto the PMMA layer. The achievement of a relatively high external quantum efficiency regardless of the emission site is the result of not only better carrier injection but also lower exciton quenching at the interface of ITO S/D electrodes, compared with metal electrodes [5]. The typical length and width were 0.1 and 2 mm, respectively.

In OLETs, the carrier transport of conjugated polymers occurs not only along the polymer chains but also between neighboring chains, and it is believed that intermolecular transport occurs via a hopping or tunneling mechanism. The copolymer SY had a glass transition temperature (T_g) of approximately 90-100 ^oC. Melting was not observed. SY OLETs with ITO S/D electrodes exhibited almost unipolar characteristics. For OLETs with SY films annealed above T_g, the hole field-effect mobility was improved. Top-gated OLETs exhibited the hole field-effect mobility of 10^{-3} – 10^{-4} $cm^2V^{-1}s^{-1}$. The hole field-effect mobility of an OLET with SY film annealed at 290 ^oC was lower than those at 150 and 200 ^oC. This result is related with the decreased π-conjugated length of SY main-chains.

An OLET based on SY film with an annealing temperature at 150 ^oC showed yellow light emission as shown in Fig. 1. Many conjugated polymers generally require high curing temperatures for OLET fabrication. The development of low-temperature-processable conjugated polymers is crucially important for fabricating printable flexible OLETs.

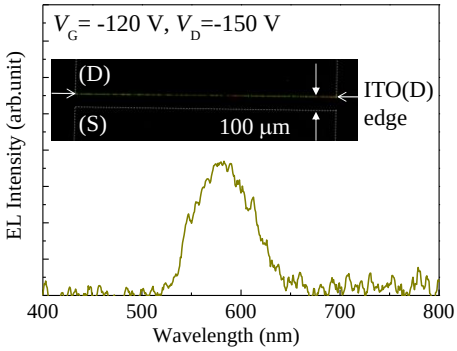

Fig. 1 EL spectrum and optical image

References

[1] S. Gambino, A. K. Bansal, I. D.W. Samuel, "Photophysical and charge-transporting properties of the copolymer Super Yellow," Org. Electron., vol. 14, pp.1980–1987, 2013.

[2] S. Burns, J. MacLeod, T. T. Do, P. Sonar, and S. D. Yambem, "Effect of thermal annealing Super Yellow emissive layer on efficiency of OLEDs," Scientific Reports, vol.7, 40805, 2017.

[3] J. S. Swensen, C. Soci, and A. J. Heeger, "Light emission from an ambipolar semiconducting polymer field-effect transistor," App. Phys. Lett. vol.87, 253511, 2005.

[4] E. B. Namdas, J. S. Swensen, P. Ledochowitsch, J. D. Yuen, D. Moses, and A. J. Heeger "Gate-Controlled Light Emitting Diodes," Advanced Materials, vol.20, pp.1321-1324, 2008.

[5] I. Ikezoe, H. Tanaka, K. Hiraoka, H. Kajii, and Y. Ohmori, "Influence of source/drain electrodes on external quantum efficiency of ambipolar organic light-emitting transistors," Org. Electron., vol.15, pp.105-110 (2014).

O4-4

Fully R2R gravure printed TFT-array for developing a digital column chromatograph

Younsu Jung[1], Hyejin Park[2], Ashish Sapkota[2], Yutaka Majima[1], and Gyoujin Cho[2]

[1]Laboratory for Materials and Structures, Tokyo Institute of Technology, Yokohama, 226-8503, Japan
[2]Department of Printed Electronics Engineering, Sunchon National University, Jeollanam-do, 57922, Korea
E-mail:jung.y.ab@m.titech.ac.jp

Organic thin film transistor (OTFT) especially based on small molecule or conducting polymer have attracted much attention in a variety of applications due to the merits of low cost and ease of fabrication. As a result, TFT related researches have been actively studied for last few decades, and it is now widely regarded as one of the most active fields as electronic devices. Since OTFT is basically an electronic device, it is usually used as basic circuits for RFID [1], flash memory [2] and active matrix backplane [3]. Moreover, it can be applied in sensor applications due to their chemical specificity of semiconductor materials which responded to target materials leading to change of electronic properties of TFT. However, OTFT based organic semiconductor materials are mostly unsuitable under atmosphere because they are very sensitive to moisture especially O_2 or H_2O molecules causing TFT performance collapse. Furthermore, since a special treatment process such as a glove box to prevent H_2O molecule is usually required in manufacturing the TFT sensor devices or in use, the mass production process (such as roll to roll (R2R) gravure printing [4]) is also not suitable to make TFT sensor devices. For this reason, single wall carbon nanotubes (SWNTs) as semiconducting material have been attracted for mass printing production process. It can easily improve their sensitivity or selectively by adopting layers. In this study we suggested a novel portable SWNTs-TFT sensor which can detect two or more kinds of chemicals at fluid state rather than a stationary state in real-time without external specific detecting systems so called “printed SWNT-TFTs array based digital column chromatography” Through R2R gravure printing process, we will discuss about fabrication, sensing mechanism and characterization for portable SWNT-TFT based automated column chromatography (Fig 1) with array structure.

This study was supported by BK Plus program, Basic Science Research (NRF-2014R1A6A1030419).

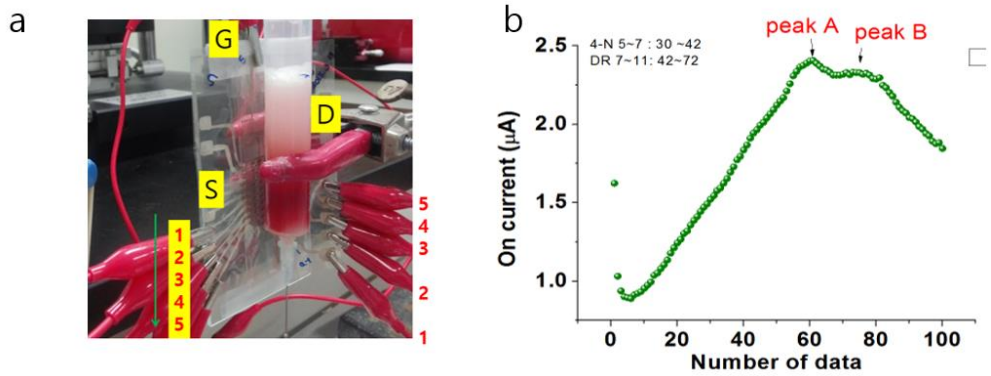

Figure 1. a) Photograph and b) performances of printed TFT array based automated column chromatography

References

[1] B. K. C. Kjellander, W. T. T. Smaal, K. Myny, J. Genoe, W. Dehaene, P. Heremans, G. H. Gelinck, “Optimized circuit design for flexible 8-bit RFID transponders with active layer of ink-jet printed small molecule semiconductors,” Org. Ele, vol.14, pp. 768-774, 2018.

[2] W. L. Leong, N. Mathews, B. Tan, S. Vaidyanathan, F. Dötz, S. Mhaisalkar, “Towards printable organic thin film transistor based flash memory devices,” J. Mater. Chem, vol. 21, pp 5203-5214, 2011.

[3] J. Sun, H. Park, Y. Jung, G. Rajbhandari, B. B. Maskey, A. Sapkota, Y. Azuma, Y. Majima, G. Cho, “Proving Scalability of an Organic Semiconductor To Print a TFT-Active Matrix Using a Roll-to-Roll Gravure,” Acs. Omega, vol. 2, pp 5766-5774, 2017.

[4] M. Jung, J. Kim, J. Noh, N. Lim, C. Lim, G. Lee, J. Kim, H. Jang, K. Jung, A. Leonard, J. Tour, G. Cho, “All-Printed and Roll-to-Roll-Printable 13.56-MHz-Operated 1-bit RF Tag on Plastic Foils,” IEEE Trans. Electron. Devices, vol. 57, pp 571-580, 2010.

O4-5

Degradation analysis of OLED by Fourier transform ion cyclotron resonance mass spectrometry imaging

Hideyuki Murata[1], Saki Shigematsu[1], Akio Miyazato[2], Keiko Miyabayashi[3], Heisuke Sakai[1]

[1] *School of Advanced Science and Technology and* [2]*Nanomaterials Technology Center*
Japan Advanced Institute of Science and Technology, Nomi, Ishikawa 923-1292, Japan
[3]*Course of Chemical and Bioengineering, Graduate School of Integrated Science and Technology*
Shizuoka University, Hamamatsu, Shizuoka 432-8561, Japan
E-mail: murata-h@jaist.ac.jp

Introduction

Many attempts to identify degradation reactions have been done by many groups with using various mass spectrometry methods [1]. Despite the improvements of mass accuracy by using better mass-scale calibration, some of the mass accuracies are not good enough for determining the unknown materials. The mass resolution of Fourier transform ion cyclotron resonance mass spectrometry (FT-ICR-MS) analysis is on the order of several tens of thousands to several hundreds of thousands, which is three order of magnitude better than that of time-of-flight (TOF) MS analysis. Thus, it is possible to distinguish constituent elements by the FT-ICR-MS. Furthermore, the mass spectrometry imaging (MSI) method, which is a method for two-dimensional mapping of mass spectrometry, allows us to visualize in-plane distribution of a substance of interest. In this study, we employ the FT-ICR-MSI to analyze degraded OLED. We have succeeded to detect the different degradation products depending on the region in the emitting area of OLED. We determined the chemical structure of the degradation product based on the analysis of accurate mass of the substance.

Experimental Section

A OLED was fabricated on an ITO substrate, on which the multi–layers consist of a molybdenum trioxide layer (MoO3) (0.75 nm), a 90 nm–thick N, N'–di–[(1–naphthaleyl)–N, N'–diphenyl]–1,1'–biphenyl–4,4'–diamine (α–NPD) and a 70 nm–thick tris (8–hydroxyquinolinolato) aluminum (III) (Alq3), lithium fluoride (LiF) (1 nm) and an aluminum layer (Al) (100 nm). The unsealed OLED was operated in a closed container filled with nitrogen gas until the luminance reached to 45% of the initial luminance. A solution obtained by dissolving degraded OLED with methanol was used for ESI-FT-ICR-MS analysis. For the FT-ICR-MSI measurement, LDI method was used to ionize the organic materials. The entire device area of 2 mm × 2 mm was scanned by a laser with a period of 50 μm. MSI-FT-ICR-MS and LDI-FT-ICR-MSI measurements were carried out using Solarix, Bruker Daltonics.

Results and Discussion

Figure 1 shows mass spectra of the extracts of pristine and degraded OLED. New peaks that only present in the degraded OLED were observed at m/z = 792.3330 (main) and 792.4110 (isotopic), which are assigned to the product generated by device operation. When a tandem MS (MS/MS) method was applied to the main peak, the fragment peak at m/z = 511.05876 arises. (Fig. 2a) Subsequently, the MS/MS measurement of the peak at m/z = 511.05876 results in the fragment peak at m/z = 367.01381. (Fig. 2b) We could not determine the chemical structure for those major fragment peaks. Since the ESI-FT-ICR-MS was carried out for the extracts from the OLEDs, a side reaction between the degradation product and the extraction solvent (MeOH) may take place during the sample preparation. Nevertheless, one of the peaks appeared at m/z = 315.07087 in the MS/MS measurement of m/z = 511.05876 was assigned to $[Alq_2]^+$ (m/z = 315.070868). From these results, we conclude that the degradation product is originated from the reaction of Alq_3.

The degraded OLED was measured using the LDI-FT-ICR-MSI method. Figure 3 shows the photograph

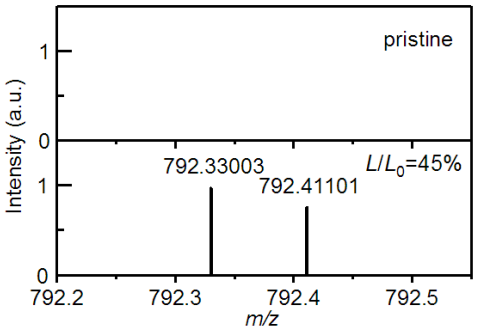

Fig. 1 ESI-FT-ICR-MS spectra of extracts of pristine (upper panel) and degraded (lower panel) OLED.

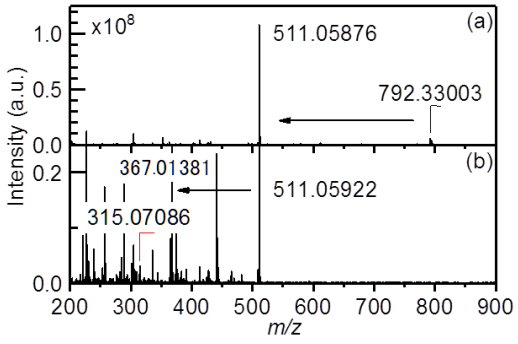

Fig. 2 ESI-FT-ICR-MS/MS spectra of extracts of degraded OLED. MS/MS spectra of the peaks at (a) m/z = 792.33003 and (b) m/z = 511.05922.

and the result of LDI-FT-ICR-MSI measured with the degraded OLED. Previously, it was reported that formation of dark spot is caused by the oxidation of Al electrode followed by the peeling off the Al electrode [2]. In other words, no degradation occurs under the dark spot. However, the characteristic peak (m/z = 772.17099) was found at the position of the dark spot in degraded OLED (Fig. 4a). This result suggests that the degradation of organic layer may occur at the dark spot area.

At the central part of OLED, where no dark spot is formed in the emitting area, the MS images of m/z = 770.15483 (Fig. 3c) coincide with the photograph of the degraded OLED. Since the mass peak at m/z = 770.15483 was mainly found in the mass spectra of the central part of degraded OLED (Fig. 4b), this mass peak was assigned to the degradation product generated during the longer device operation.

To find a molecular formula corresponding to m/z = 770.15483, we used the program (Data Analysis 4.2) equipped to the Solarix. Among the many candidate molecular formulas, $C_{45}H_{26}Al_2N_5O_5$ was mostly plausible one, error < 1.4 ppm, to the peak. This molecular formula is close to the $[Al_2q_5]^+$ ($C_{45}H_{30}Al_2N_2O_5$), which was reported as a photochemical reaction product of Alq_3 (Fig. 5a) [3]. The difference of m/z between $[Al_2q_5]^+$ (m/z = 774.187223) and the peak at m/z = 770.15483 was 4.032393, which exactly matches to the accurate mass of four hydrogens. Based on these results, we concluded that a chemical structure of $C_{45}H_{26}Al_2N_5O_5$ is the crosslinked product of the $[Al_2q_5]^+$ such as $[Al_2q_5\text{-}4H]^+$ followed by the elimination of four hydrogens. (Fig. 5b)

Summary

In this study, we demonstrate that the FT-ICR-MS method can detect the reaction products of OLED with high accuracy. We determined the chemical structure of the degradation product of Alq_3-based OLED for the first time.

References

[1] S. Schölz, *et al.*, "Degradation Mechanisms and Reactions in Organic Light-Emitting" *Chem. Rev*., vol. 115, pp. 8449-8503, 2015.

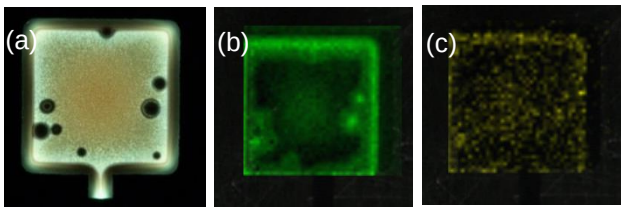

Fig. 3 (a) Photograph of degraded OLED. LDI-FT-ICR-MSIs of (b) m/z = 772.17099, (c) m/z = 770.15483

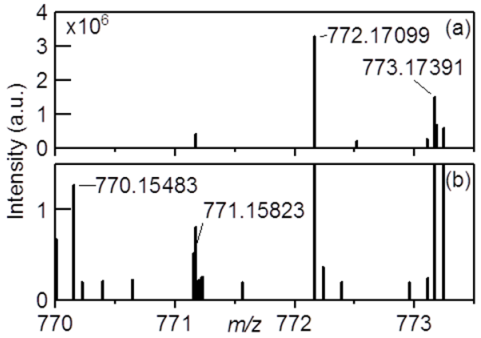

Fig. 4 LDI-FT-ICR-MS spectra of degraded OLED. (a) in dark spot area; m/z = 772.17099 (parent) and 773.17391 (isotopic), (b) in the center; m/z = 770.15483 (parent) and 771.15823 (isotopic)

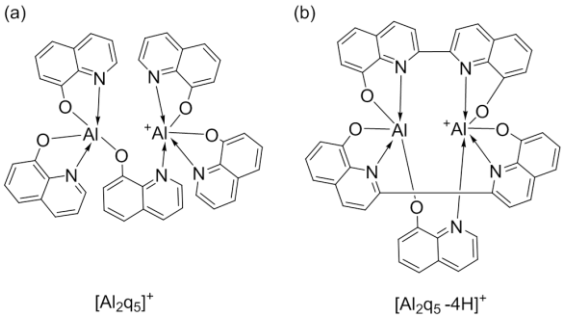

Figure 5. Chemical structures of (a) $[Al_2q_5]^+$ and (b) degradation product $[Al_2q_5\text{-}4H]^+$

[2] M. Schaer, *et al.*, "Water vapor and oxygen degradation mechanisms in organic light emitting diodes,"*Adv. Func. Mater*, vol.11, no. 2, pp. 116-121, 2001.

[3] S. Schölz, *et al.*, "Photochemical reactions in organic semiconductor thin films" *Org. Electron*.,vol. 8, pp. 709-717, 2007.

O4-6

Hole transport property of α-phenyl-4'-(diphenylamino)stilbene single crystal prepared based on solubility and supersolubility curves

Mitsuhiko Katagiri,[1] Shofu Matsuda,[1] Norio Nagayama,[1,2] Minoru Umeda[1,*]

[1]*Department of Materials Science and Technology, Nagaoka University of Technology, Kamitomioka, Nagaoka, Niigata 940-2188, Japan*
Tel: + 81 - 258 - 46 - 6000, Fax: +81 - 258 - 47 - 9300
[2]*Ricoh Company, Ltd., Izumi, Ebina, Kanagawa 243-0460, Japan*
Tel: + 81 - 46 - 236 - 2400
E-mail: mumeda@vos.nagaokaut.ac.jp

Anisotropic carrier transport has been studied at a surface of triphenylamine-derivative single crystal prepared in a tetrahydrofuran (THF) solution. Triphenylamine derivatives are commonly used as a hole-transport material for organic photoconductors of laser-beam printers [1]. In the devices, the materials are used as an amorphous form, in which charge carrier mobility is in the order of ~10^{-4} $cm^2V^{-1}s^{-1}$. For realizing a further high mobility as an organic semiconductor, preparation of a single crystal seems to be a promising way [2,3]. In this study, a single crystal of a α-phenyl-4'-(diphenylamino)stilbene (TPA) was prepared based on solubility and supersolubility curves. Then, its anisotropic carrier transport properties were measured.

First, the solubility and supersolubility curves were measured employing THF solvents of the TPA. The results are shown in Fig. 1. Based on the results, a single crystal preparation was conducted using a 40 wt.% TPA solution with a cooling rate of 0.5 °C/day started from 35 °C for 48 h, resulted in a crystal of 7.0 x 0.9 x 0.8 mm as seen in Fig. 2. A polarizing microscope observation demonstrated an extinction angle, which ensures that a single crystal of the TPA was obtained.

Next, current-voltage properties of the single crystal were measured in a vacuum chamber connected to a source meter (Keythley 2612A). For the measurement, Au parallel electrodes with a distance of 10 μm were vacuum deposited on the surface of the crystal. Fig. 3 shows an electric-field dependency of the currents obtained in long-axis, short-axis, and thickness directions. From Fig. 3, the long-axis current is larger than those of the short-axis and the thickness, which reveals anisotropic surface charge transports occur at the single crystal. This can be well explained by a molecular orientation of the prepared TPA crystal structure.

References

[1] T. Niimi, M. Umeda, "Electron transfer between a photoexcited azo pigment particle and an electron donor molecule in a solid system," *J. Phys. Chem. B*, 106, 3657–3661 (2002).
[2] M. Umeda, M. Katagiri, S. Shironita, N. Nagayama, "Anisotropic surface hole-transport property of triphenylamine-derivative single crystal prepared by a solution method," *Appl. Surf. Sci.*, 338, 109–113 (2016).
[3] M. Kunihiro, Y. Nakasone, S. Matsuda, S. Shironita, N. Nagayama, M. Umeda, "Crystal structure oriented carrier transport characteristic of triphenylamine derivative single crystal," *AIP Adv.*, 8, 035324, (2018).

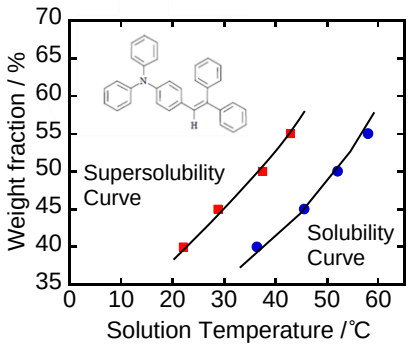

Fig. 1 Solubility and supersolubility curves of TPA-THF solution. Inset shows TPA molecular structure.

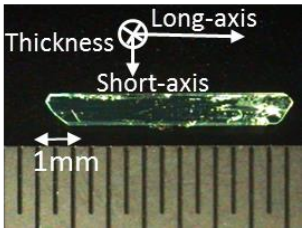

Fig. 2 Photograph of TPA single crystal.

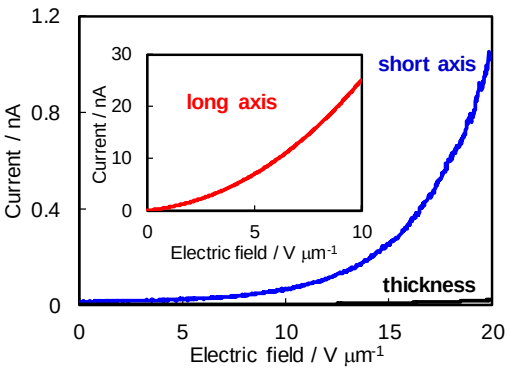

Fig. 3 *i-E* characteristics in long-axis, short-axis, and thickness directions of the obtained TPA single crystal.

O4-7

Low-cost fabrication of polymer electronic devices employing the eco-friendly push-coating process

Varun Vohra,[a] Shusei Inaba,[a] Francesco Galeotti,[b] Umberto Giovanella[b] and Chiara Botta[b]

[a] *Department of Engineering Science, University of Electro-Communications, 1-5-1 Chofugaoka, Chofu, Tokyo, 182-8585 Japan*
Tel: + 81 - 42 - 443 - 5359, Fax: + 81 - 42 - 443 - 5359
E-mail: varun.vohra@uec.ac.jp
[b] *Institute for Macromolecular Science (ISMAC-CNR), Via Alfonso Corti, 12, Milano, 20133, Italy*

(1) Introduction

Polymer light-emitting devices (PLEDs) and polymer solar cells (PSCs) have a promising potential for low-cost production or electronic devices by solution processes such as spin-coating. Over the past few years, the power conversion efficiencies (PCEs) of PSCs and the external quantum efficiencies (EQEs) of PLEDs have rapidly improved with values now regularly over 10%.[1,2] Nonetheless, the PSC active layers and the PLED emitting layers are commonly deposited using spin-coating from chlorinated aromatic solvents such as chlorobenzene (CB) or dichlorobenzene (DCB) which are harmful to the environment and can damage organs such as the lungs, the kidney or the central nervous system as well as increase fetal mortality. Spin-coating generates a large amount of hazardous solvent and active material wastes which considerably increases the cost of production (including the cost necessary for proper disposal of the solvent). Therefore, one of the major issues to solve before solution-processed organic electronic technologies can be commercialized on a large scale is to find alternative deposition techniques which can considerably reduce the materials waste during thin film formation. In 2012, Ikawa *et al.* introduced a process called push-coating in which a polydimethylsiloxane (PDMS)-based thin layer is deposited on small amounts of conjugated polymer solutions to form highly uniform thin films on large areas.[3] A thin wet film is formed by capillary forces spreading the solution between the substrate and the PDMS layer. The solvent then slowly diffuses into PDMS to form uniform thin films and enable simple recovery and recycling of hazardous solvents (Figure 1). Although push-coating was successfully applied to high efficiency field-effect transistors production, employing this green process for PSC active layer deposition resulted in large decreases in PCE as compared to conventionally deposited (spin-coated) devices.[4]

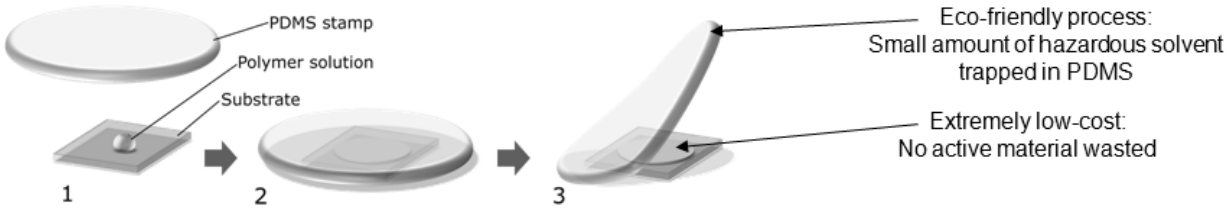

Figure 1. Schematic representation of the push-coating process.

Here, we introduce our study on push-coating employing mm-thick PDMS films to fabricate efficient or original PLEDs and PSCs. In particular, we demonstrate that thicker PDMS films have several advantages with respect to ultrathin (~ 100 nm) films previously employed for PSC fabrication. They enable easy handling, have adequate solvent retention properties to recycle hazardous solvents and remove the necessity to use additional weight during push-coating. Consequently, PLEDs and PSCs with similar performances to spin-coated ones can be fabricated using 20 times less solvent and active materials.[5] Furthermore, nanostructured PDMS can be produced using self-assembled nanoporous templates and they can be employed for the fabrication of nanopixel PLEDs by push-coating.[6]

(2) Efficient PSCs fabricated through the eco-friendly push-coating process

To verify whether push-coating can be employed for efficient PSC production, we first fabricated regular devices with the state-of-the-art active layer materials, namely, P3HT:$PC_{61}BM$, in regular device architectures (ITO/PEDOT:PSS/active layer/LiF/Al). In push-coated active layers, a clear increase in polymer crystallinity can be observed with respect to spin-coated ones. In fact, similar crystallinities are obtained for push-coated devices produced at 50°C (5 min) and spin-coated devices post-annealed at 140°C (10 min) when DCB is employed as the solvent. Push-coating is a slow drying process which provides enough time for the polymer chains to arrange into highly organized structures. Annealed spin-coated and unannealed push-coated P3HT:$PC_{61}BM$ active layers produce similar PCEs of 3.3% in regular device architectures (Figure 2). We then verified whether push-coating can be employed to fabricate higher efficiency PSCs. For that purpose, we used active solutions composed of PCDTBT:$PC_{71}BM$ in an inverted device architecture (ITO/ZnO/active layer/MoO_3/Ag). Once again, devices fabricated by spin-coating and push-coating yield similar PCEs of 5.2% with only 2μl of active layer solution used in the case of push-coating (~100μl for spin-coating).

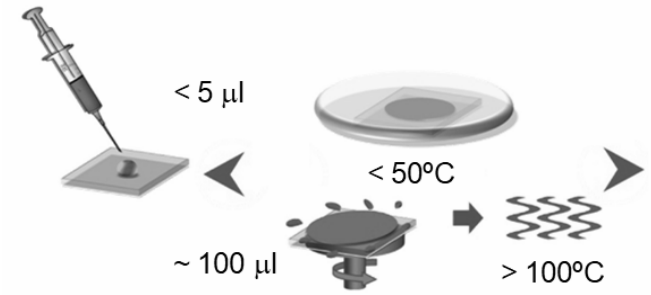

	Jsc (mA cm^{-2})	Voc (mV)	FF (%)	PCE (%)
P3HT:PC_{61}BM Spin-coating	8.34	608	65.0	3.30
P3HT:PC_{61}BM Push-coating	8.46	589	67.2	3.34
PCDTBT:PC_{71}BM Spin-coating	11.28	884	52.2	5.20
PCDTBT:PC_{71}BM Push-coating	10.58	910	53.7	5.16

Figure 2. Comparison of process parameters (amount of solution, temperature) and device performances of spin-coated and push-coated PSCs.

(3) Flat and nanostructured PLEDs produced by push-coating

Recent results on F8BT-based PLEDs suggest that their EQEs can be enhanced by using thick emitting layer.[2] Nonetheless, due to the limited solubility of conjugated polymers in organic solvents, spin-coating thick uniform emitting layers can become highly challenging. We verified the effect of emitting layer thickness on the EQEs of unannealed push-coated F8BT PLEDs and compared them to the device performances of unannealed and annealed spin-coated PLEDs (Figure 3a). Although the EQE of unannealed spin-coated PLEDs decreases with increasing thickness, annealing at high temperatures of 150°C can improve their performances. On the other hand, high polymer crystallinities are obtained in as-deposited push-coated F8BT films, which enable the fabrication of 350 nm-thick emitting layers producing high EQEs without annealing (EQEs 20% higher than the best annealed spin-coated devices). Additionally, using self-assembled templates, we developed a low-cost nanofabrication technique to produce nanopixel PLEDs (nano-push-coating).[6] The nanoporous F8BT films fabricated using nano-push-coating exhibit ring-like photoluminescence and hexagonally arranged nanopixel electroluminescence resulting from the stronger electric field generated in the thinner emitting layer at the center of the pores (Figure 3b).

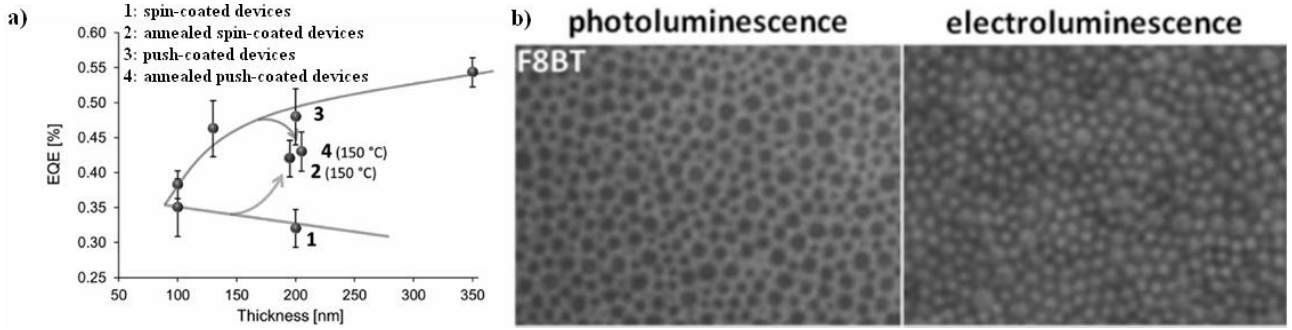

Figure 3. a) EQEs of spin-coated and push-coated F8BT PLEDs; **b)** photoluminescence and electroluminescence of nano-push-coated F8BT emitting layers.

(4) Conclusions

In summary, we were able to demonstrate that employing thick PDMS layers is the key to produce efficient PSCs and PLEDs. Unlike spin-coated polymer films which require high temperature annealing to produce crystalline layers, as-deposited push-coated active and emitting layers exhibit high crystallinities and device performances. PSCs with PCEs up to 5.2% were fabricated using inverted device architectures and we expect to produce devices with PCEs over 10% in the near future. Thick push-coated PLEDs demonstrate higher EQEs compared to spin-coated devices. Nanostructured PDMS can be employed to produce PLEDs in which electroluminescence is observed from hexagonally arranged nanopixels. This versatile deposition process which can be applied to virtually any conjugated polymers opens the path to remarkably low-cost fabrication of devices with extremely low environmental impact.

References

[1] V. Vohra *et al.* "Efficient inverted polymer solar cells employing favourable molecular orientation," Nat. Photonics, vol. 9, pp. 403-408, May 2015.

[2] B.R. Lee *et al.* "Highly efficient inverted polymer light-emitting diodes using surface modifications of ZnO layer," Nat. Comm., vol. 5, pp. 4840, September 2014.

[3] M. Ikawa *et al.* "Simple push coating of polymer thin-film transistors," Nat. Comm., vol. 3, pp. 1176, November 2012.

[4] S. Kobayashi *et al.* "Bulk heterojunction organic solar cells fabricated using the push coating technique," J. Chinese Adv. Mater. Soc., vol. 3, pp.1-8, October 2014.

[5] V. Vohra *et al.* "Low-Cost and Green Fabrication of Polymer Electronic Devices by Push-Coating of the Polymer Active Layers," ACS Appl. Mater. Interfaces, vol. 9, pp. 25434-25444, July 2017.

[6] V. Vohra *et al.* "Nanostructured light-emitting polymer thin films and devices fabricated by the environment-friendly push-coating technique," ACS Appl. Mater. Interfaces, *in press*.

O4-8

Impact of orientation polarization on electron injection in OLED studied by negative ion photoemission spectroscopy and displacement current measurement

T. Makino[1], H. Kinjo[1], Y. Tanaka[1,2], and H. Ishii[1,2,3]

[1]Graduate School of Advanced Integration Science, [2]Center for Frontier Science, [3]Molecular Chirality Research Center, Chiba University, 1-33 Yayoi-cho, Inage-ku, Chiba-shi 263-8522 Japan
Tel: + 81 - 43 - 290 - 3524, Fax: +81- 43 -290 - 3523
E-mail:ishii130@faculty.chiba-u.jp

Many organic EL materials show more or less spontaneous orientation polarization in their evaporated films with giant surface potential (GSP)[1]. The observed potential across the film is often comparable to the driving voltage of organic light-emitting diodes (OLEDs). This polarization induces positive and negative fixed charges on both ends of the polarized layer, leading to interface charges at organic/organic and organic/electrode interfaces in OLEDs. The positive interface charges near the cathode has been expected to assist electron injection by attracting negative carriers, but this effect is not directly verified. In this study, the impact of orientation polarization on electron injecting nature was investigated from the viewpoints of their electronic structures and carrier behavior.

Regarding electronic structure, anion states of several OLED materials with GSP (Alq_3, TPBi, α-NPD, and 4CzIPN) were investigated by high-sensitivity ultraviolet photoemission spectroscopy (HS-UPS) and photoelectron yield spectroscopy (HS-PYS). As shown in Fig.1, PYS spectra of these materials show lower energy onset than conventional ionization energy (black triangles). HS-UPS spectra also show lower energy onset (blue arrows); their onset energies are 2-3 eV. This low energy photoemission can be ascribed to the photoemission from the anion captured by positive polarization charge at the surface. It should be noted that the observed onsets of HS-PYS and HS-UPS tend to be deeper than the affinity levels from inverse photoemission spectroscopy in literature. The difference is roughly 1 eV at most. We conclude the Coulomb interaction between the anion and the polarization charge due to GSP energetically stabilize the anion states and make the LUMO deeper with lower injection barrier [2].

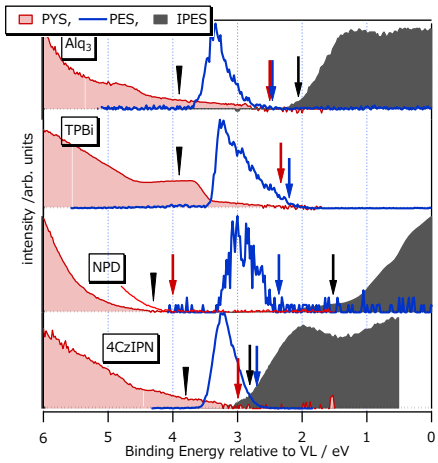

Fig.1 PYS and HS-UPS spectra of Alq_3, TPBi, α-NPD, and 4CzIPN films with IPES spectra from literatures

Regarding carrier behaviour, OLED performance of ITO/α-NPD/Alq_3/Al and ITO/α-NPD/Al(7-prq)$_3$/Ca devices was investigated. Al(7-prq)$_3$ is a derivative of Alq_3; the position 7 of quinolinol group is replaced by propyl group. These two molecules show opposite polarity of polarization; the cathode side of Alq_3 has positive interface charge, but negative for Al(7-prq)$_3$. Voltage-current characteristics revealed higher current for Alq_3 device, suggesting lower contact resistance at Alq_3/Al interface [3]. To clarify this point, displacement current measurement (DCM), in which current is measured under a triangular voltage scan, was performed for *electron only* device (EOD) of ITO/$C_{44}H_{90}$/Alq_3/Al and ITO/$C_{44}H_{90}$/Al(7-prq)$_3$/Al as shown in Fig.2. Before DCM measurement, the polarization charge near $C_{44}H_{90}$/(Alq_3 and Al(7-prq)$_3$) interfaces by illuminating the device, and then electron injection from Al electrode was investigated. The threshold voltage where the displacement current showed to increase due to electron injection (labeled by vertical arrow) was found to shift toward much higher voltage side for Al(7-prq)$_3$ device, clearly indicating that positive interface charge near the cathode supports electron injection, while negative charge increases the resistance.

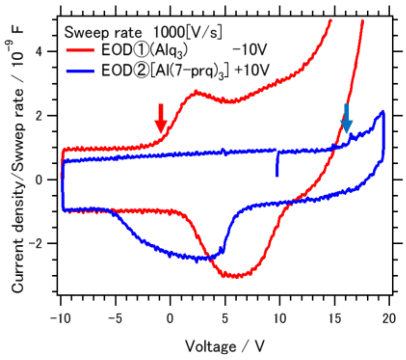

Fig.2 DCM curves of two electron only MIS device of Alq_3 and Al(7-prq)$_3$.

The above examination on the basis of electronic structure and carrier behavior clearly demonstrate the impact of orientation polarization on electron injection. The control of this phenomenon is a key to get good electron injection nature in various organic electronics including not only OLED but also organic transistors etc.

References

[1] Y. Noguchi, Y. Miyazaki, Y. Tanaka, N. Sato, Y. Nakayama, T. D. Schmidt, W. Brütting, and H. Ishii, "Charge accumulation at organic semiconductor interfaces due to a permanent dipole moment and its orientational order in bilayer devices", Journal of Applied Physics, vol. 111, no. 11, pp. 114508-1～10, June 2012.
[2] H. Kinjo, H. Lim, T. Sato, Y. Noguchi, Y. Nakayama and H. Ishii, "Significant relaxation of residual negative carrier in polar Alq_3 film directly detected by high-sensitivity photoemission", Applied Physics Express, vol. 9, no. 2, pp.021601-1~4, January 2016.
[3] Y. Noguchi, H. Lim, T. Isoshima, E. Ito, M. Hara, W. W. Chin, J. W. Han, H. Kinjo, Y. Ozawa, Y. Nakayama, and H. Ishii, "Influence of the direction of spontaneous orientation polarization on the charge injection properties of organic light-emitting diodes", Applied Physics Letters, vol. 102, no.20, pp.203306-1~5, May 2013.